Biophysical Chemistry 143 (2009) 1–17

Contents lists available at ScienceDirect

Biophysical Chemistry

journal homepage: http://www.elsevier.com/locate/biophyschem

Mathematical model of NO and O_2 transport in an arteriole facilitated by hemoglobin based O_2 carriers

Sharon Irene Gundersen, Guo Chen, Andre Francis Palmer *

The Ohio State University, Department of Chemical and Biomolecular Engineering, 140 West 19th Avenue, Columbus, OH 43210, United States

ARTICLE INFO

Article history:
Received 6 January 2009
Received in revised form 10 February 2009
Accepted 10 February 2009
Available online 21 February 2009

Keywords:
Nitric oxide
Oxygen transport
Hemoglobin-based oxygen carriers
Arteriole transport
Vasoconstriction
Microcirculation

ABSTRACT

The increasing demand for donated human blood has spurred research to develop hemoglobin-based O_2 carriers (HBOCs) that can be used as red blood cell (RBC) substitutes. However, *in vivo* studies of acellular HBOCs have shown an increase in mean arterial pressure following transfusion that has been attributed to the HBOC's ability to scavenge NO (an important vasodilator that is synthesized by endothelial cells in the blood vessel wall that signals neighboring smooth muscle cells to relax). In this study, a mathematical model was developed to describe NO and O_2 transport in an arteriole containing a mixture of acellular HBOCs and RBCs. The acellular HBOCs studied in this work possessed a wide range of O_2 affinities, O_2 dissociation rate constants and NO reactivities in order to evaluate their effect on O_2 tension and NO concentration in the arteriole tissue region. By focusing on the concentration of NO that is localized in the arteriole smooth muscle cell region, the model can predict the vasopressor response of HBOCs. The results of this study confirmed that acellular HBOCs scavenge large amounts of NO from the entire arteriole (~50% or more NO compared to RBCs only). A recombinant Hb, rHb3011, displayed the least NO reactivity and consequently left the most NO remaining in the arteriole. The NO concentration in the arteriole with respect to the other HBOCs studied was proportional to their NO reactivity. Therefore, the results of this study demonstrate that NO scavenging is an unavoidable consequence of transfusing HBOCs. To prevent or reduce vasodilatation, we suggest administration of NO by either inhaling NO or transfusing nitrite into the blood stream followed by transfusion of HBOC.

1. Introduction

Due to the increasing demand on donated human blood for various transfusion applications, work is being done to develop hemoglobin-based oxygen carriers (HBOCs) as an alternative to donated red blood cells (RBCs). However, the majority of clinical studies on acellular HBOCs have observed an increase in mean arterial pressure (MAP) following transfusion of HBOCs into the systemic circulation [1–5]. It is hypothesized that this side-effect is due to the enhanced ability of acellular HBOCs to scavenge NO as it is readily dispersed in the plasma layer of arterioles and hence closer to the source of NO generation (endothelial cells).

NO is an important regulatory molecule in the cardiovascular system. NO plays key roles in regulating blood flow, platelet aggregation, leukocyte adhesion, host defense responses and smooth muscle tone [6–9]. In response to a variety of stimuli, NO is generated by endothelial cells in the blood vessel wall from the enzymatic degradation of L-arginine by NO synthase [7,8,10]. It passively diffuses out of the vessel wall, where it is rapidly consumed by several chemical reaction pathways [6]. NO activates soluble guanylate cyclase (sGC) in smooth muscle cells resulting in vasorelaxation [6,8,11–13]. NO also rapidly reacts with heme containing proteins such as hemoglobin (Hb) that is contained within RBCs, or myoglobin (Mb) in muscle tissue. NO will irreversibly bind with deoxyHb or will oxidize HbO_2 to yield methemoglobin (metHb) and NO_3^- [4]. Therefore, heme proteins function as an NO sink. In addition, NO can be consumed by tissues and oxidized by super oxide [6,8].

Although heme proteins behave as a NO sink, the blood vessel wall and surrounding tissue space are not void of NO, since NO's reaction rate with Hb that is contained inside RBCs is 2–3 orders of magnitude slower compared to an equivalent amount of acellular Hb [7,8]. This vast difference in reaction rate has been attributed to two main hypotheses: 1) The plasma layer surrounding individual RBCs is "unstirred" which results in an increase in the diffusion resistance of NO; 2) The RBC membrane itself acts as a diffusional barrier to NO, especially the cytoskeleton and oxidized Hb (metHb) [7].

Therefore, understanding the effect of transfused HBOCs on the local NO concentration in an arteriole can be very beneficial in optimizing further development of HBOCs that mitigate the hypertensive effect. In this study, O_2 and NO transport in an arteriole was

* Corresponding author. Tel.: +1 614 292 6033; fax: +1 614 292 3769.
E-mail address: palmer.351@osu.edu (A.F. Palmer).

0301-4622/$ – see front matter © 2009 Elsevier B.V. All rights reserved.
doi:10.1016/j.bpc.2009.02.005

mathematically modeled, with and without HBOCs, in order to examine the effect of the various HBOCs on the local O_2 and NO tension. An ideal HBOC should supply sufficient O_2 to surrounding tissues to ensure their normal function, while maintaining NO levels high enough in smooth muscle cells to facilitate vascular relaxation via sGC activation. The exact EC_{50} for NO activation of sGC is not fully understood, with literature values ranging from 2.9 to 1600 nM as summarized by Chen et al. [14]. One study by Condorelli et al. simulated the kinetics of sGC activation, and their calculated value of 23 nM is used as a point of reference in the discussion section of this work [6].

More specifically, this study simulated O_2 and NO transport in an arteriole exposed to a mixture of RBCs with five different types of acellular HBOCs having a wide range of molecular diffusivity, oxygen affinity, oxygen dissociation kinetics and NO reactivity. The physical properties of the HBOCs used in this theoretical study are listed in Table 1. MP4 consists of human Hb conjugated with an average of six maleimide-activated polyethylene glycol chains per Hb tetramer with an average molecular weight of 95 kDa [1,15–17]. PolyBvHb consists of a glutaraldehyde polymerized bovine Hb with an approximate molecular weight of 336 kDa [18,19]. Two recombinant Hbs were also included in this study, rHb 3011 and rHb 1.1, which are described in previous studies [3,4,20]. All of these HBOCs were compared to the O_2 transporting ability and NO scavenging potential of wild type human Hb (wt Hb) and hamster RBCs [21]. It is important to note that *in vivo* administration of unmodified wt Hb is not practical, since the tetramer can dissociate into αβ dimers, is toxic to tissues and can lead to renal failure [5,22].

The physical properties of various HBOCs are listed in Table 1 along with their P_{50} (i.e. oxygen affinity, which corresponds to the pO_2 at which the HBOC is half-saturated with O_2) and cooperativity coefficient (n). It is important to note that the cooperativity of bovine Hb derived HBOCs (e.g. PolyBvHb) is allosterically regulated by the chloride ion concentration. The reported P_{50}s and cooperativities in Table 1 were determined at physiological temperature (37 °C), pH, and chloride ion concentration. Significant changes in these conditions would alter the P_{50} and cooperativity of the HBOCs and thus affect O_2 transport. Table 1 also includes the HBOC's diffusion coefficient (D_{HBOC}), O_2 dissociation rate constant (k_{HBOC-}), and NO association rate constant ($k_{NO-HBOC}$). The diffusion coefficient of RBCs refers to the diffusivity of Hb that is contained within the RBC and is a function of Hb concentration.

The O_2–HBOC/RBC equilibrium curve of each HBOC/RBC is displayed in Fig. 1-A. Curves that are shifted to the left represent a decrease in P_{50} and an increase in O_2 affinity. In this figure, the P_{50} ($Y=0.5$) is located near the region of maximum slope, dY/dpO_2, on the curve. The first derivative of the O_2–HBOC/RBC equilibrium curve with respect to pO_2 is displayed in Fig. 1-B where the maximum slope occurs near the P_{50}.

Table 1
Physical properties of HBOCs used in the transport simulations.

HBOC	P_{50} (mm Hg)	n	D_{HBOC} (cm^2/s)	k_{HBOC-} (1/s)	$k_{NO-HBOC}$ (1/μM/s)	Description
MP4	5.53	1.25	4.49×10^{-7}	60	22	Maleimide-activated poly(ethylene glycol)-conjugated human Hb [15–17]
rHb 1.1	32	2.3	6.23×10^{-7}	66.5	80.92	Recombinant human Hb [3,4]
rHb 3011	46	1.3	6.23×10^{-7}	24.3	2.3	Recombinant human Hb [3,4]
PolyBvHb	35.1	1.4	2.91×10^{-7}	62	15	Glutaraldehyde polymerized Hb [18,19]
wt Hb	12.04	2.4	6.23×10^{-7}	23.12	60	Wild type Hb [4]
RBCs	29.3	2.2	f([Hb])	44	0.14 [23]	Hamster RBCs [21]

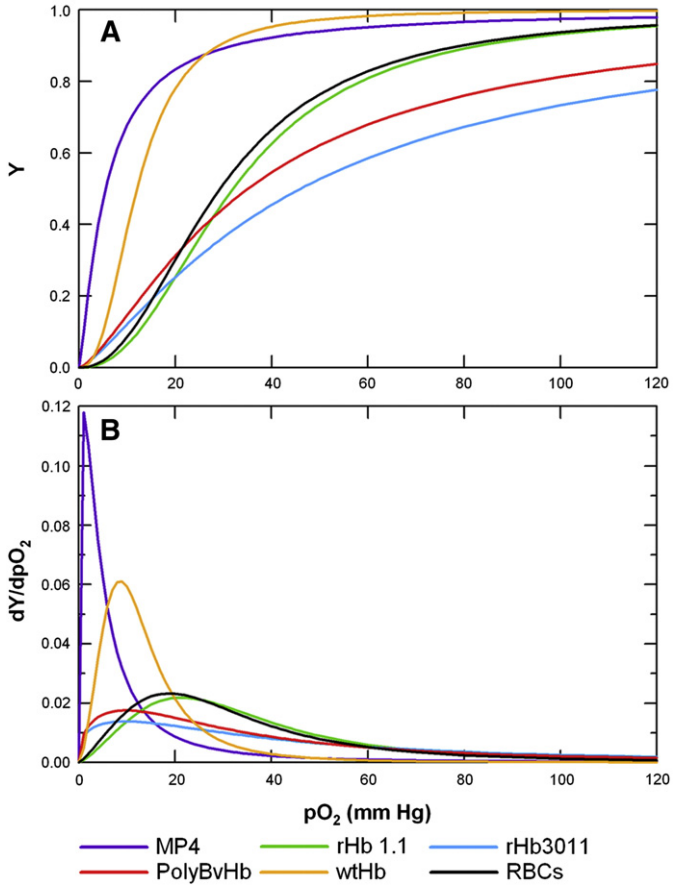

Fig. 1. A) O_2–HBOC/RBC equilibrium curves of all HBOCs/RBCs simulated in the O_2–NO transport model. Most of the curves were generated using the Hill equation (Appendix D) and P_{50} and cooperativity listed in Table 1, except for the O_2–RBC curve which was generated using the overall Adair equation (Appendix D) and the Adair constants listed in Table 2. B) First derivative, or slope, of the O_2–HBOC/RBC equilibrium curves shown in Part A. dY/dpO_2 has units of [1/mm Hg].

The O_2–NO transport model described in this work differs from other models of O_2–NO transport in several ways. First, it omits the assumption of instantaneous equilibrium between O_2 and Hb/Mb. Instead it accounts for the reaction kinetics between O_2 and Hb/Mb as described in previous studies [21,24,25]. The rate of NO consumption by heme groups (in Hb or Mb) is mathematically described by a simple kinetic rate law with experimentally determined rate constants for each HBOC and is dependent on the local heme concentration. The model also considers NO consumption by Mb, and compares the effect of Mb in the tissue space on pO_2 and NO concentration ([NO]). Two stagnant cell free layers are included in the model: the protein glycocalyx layer lines the inside of the blood vessel wall and an interstitial region exists between the vessel wall and the smooth muscle region. Finally, the model considers the axial diffusion of dissolved gases and Hb along the length of the arteriole (although this effect is negligible).

As established in many previous studies, this model subdivides the lumen of the arteriole into two regions: a RBC-rich core region and a cell-depleted plasma region that exists between the core and glycocalyx layer [7,9,23]. RBC suspensions flowing in arteriole sized tubes will migrate toward the axial centerline via shear-induced migration and form a RBC-rich core and a concentric cell-depleted plasma region near the vessel wall [26–30]. This phenomena causes the majority of RBCs to exist in a higher viscosity and higher hematocrit (*hct*) core region and creates an additional plasma region that NO and O_2 must diffuse through. The fraction of the total arteriole lumen radius that is composed of this core region is a function of the blood *hct* and arteriole lumen radius [31,32].

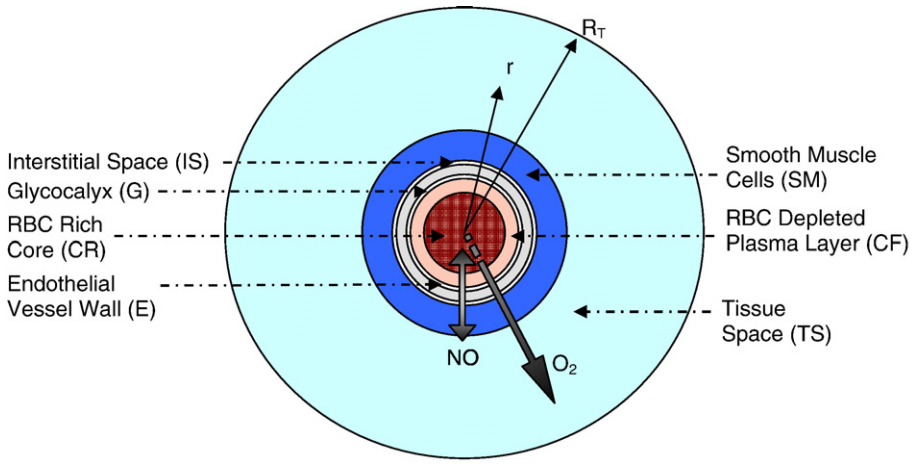

Fig. 2. Schematic cross-section of the modified KTC model geometry delineating each subregion: RBC-rich core region (CR), RBC-depleted plasma layer (CF), glycocalyx (G), endothelial vessel wall (E), interstitial space (IS), smooth muscle cells (SM) and tissue space (TS).

The current model will use a blunted *hct* and velocity profile as developed by Chen et al. [27]. Although the previous group evaluated three possible *hct* and velocity profiles, they reported that their linear profile may be a closer representation to *in vivo* conditions and therefore will be the only profile used in the current study.

Although most physiological scenarios were simulated at normal tissue pO_2s, hypoxic pO_2s were included to simulate a range of oxygenation situations that could arise due to blood loss. A range of inlet pO_2s ranging from 5 to 115 mm Hg was used to study the effect of the HBOC's physical properties on the dissolved O_2 and NO concentration profile in the arteriole, percentage of incoming O_2 consumed by the tissues, and overall O_2 transfer rate (k_o). The *hct* was also varied to examine O_2 and NO transport under various degrees of blood loss: 45%, average normal blood volume; 35%, one-fourth of total blood

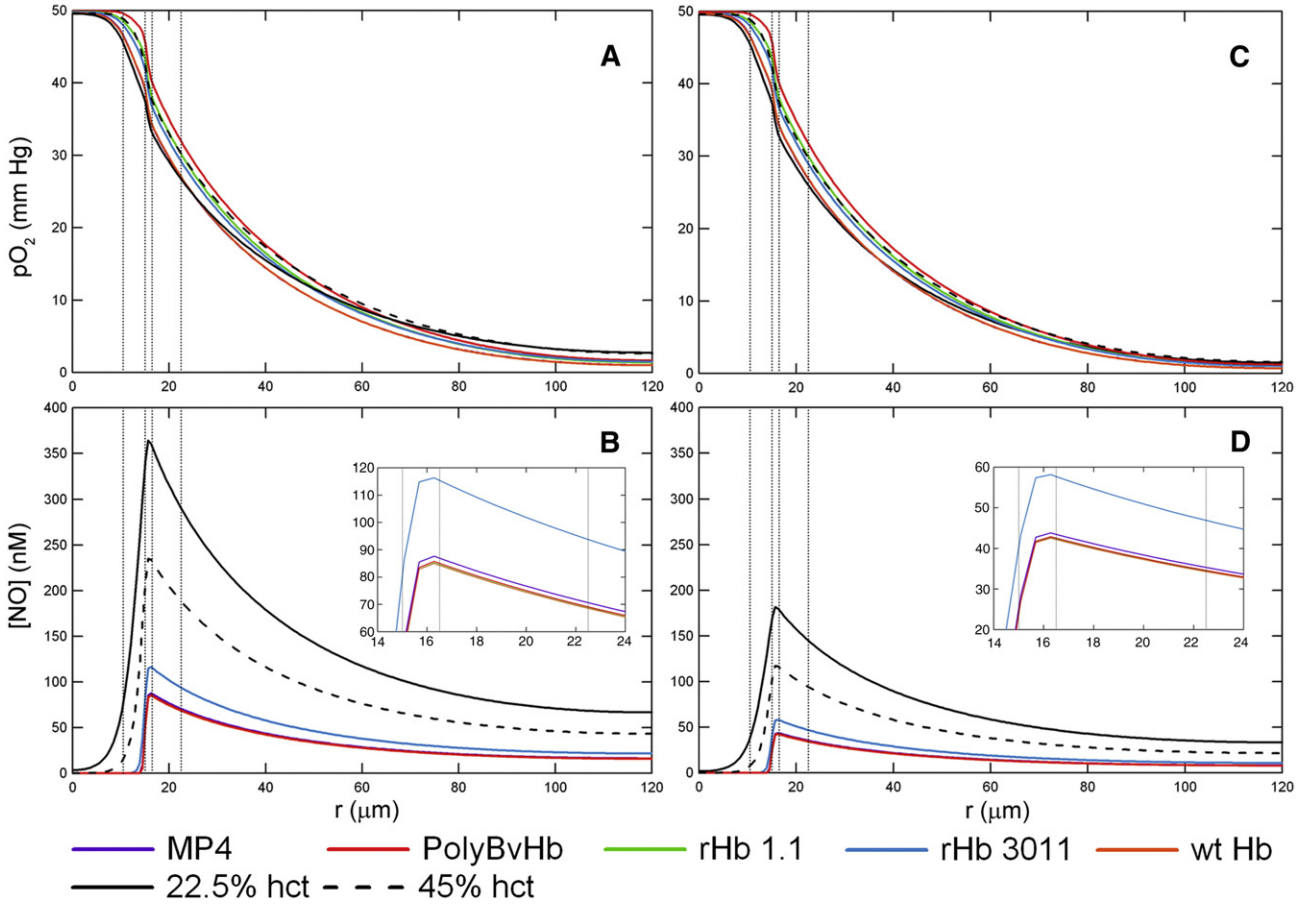

Fig. 3. O_2 tension profiles are shown at a *hct* of 22.5%, inlet $pO_2 = 50$ mm Hg without Mb in the tissue space at A) $R_{NO,max} = 300$ μM/s and C) $R_{NO,max} = 150$ μM/s. The corresponding [NO] profiles are shown at B) $R_{NO,max} = 300$ μM/s and D) $R_{NO,max} = 150$ μM/s. Transfusion of HBOCs replaced the lost RBC heme concentration to 22.5% *hct* (50% blood loss). The vertical lines represent the interface between the RBC-rich core region, RBC-depleted plasma layer and glyocalyx, endothelial vessel wall, interstitial space and smooth muscle cells, and tissue space.

volume is lost; and 22.5%, half of total blood volume is lost. Finally, two endothelial cell NO production rates were simulated to cover the range of available literature values [27].

The O_2 and NO transport model described herein is a modification of the Krogh tissue cylinder (KTC) model for a single arteriole [24,25,33,34]. A schematic radial cross-section of the model geometry is shown in Fig. 2. It consists of: 1) a red blood cell-rich core (CR); 2) a red blood cell-depleted plasma layer (CF); 3) a stagnant protein glycocalyx layer (G); 4) endothelial vascular wall (E); 5) cell-free interstitial space (IS); 6) smooth muscle layer (SM) and 7) tissue space (TS). The modified KTC model was simulated using Comsol Multiphysics (Comsol, Burlington, MA) using the Chemical Engineering Expansion Pack Add-In for an axial symmetric mode. The model solves for the following five parameters: dissolved O_2 (pO_2), dissolved NO, fraction of O_2 saturated Hb contained within RBCs (S_{RBC}), fraction of O_2 saturated Hb contained within HBOCs (S_{HBOC}), and fraction of O_2 saturated Mb (S_{Mb}). The governing equations describing this transport model are derived in Appendix A. The Appendices also contain explanations of the flow through each region and the governing equations for fluid flow and hct profile (RBC distribution).

2. Results

2.1. O_2 and NO profiles

Fig. 3 shows the radial pO_2 and [NO] profiles at the axial midpoint of the arteriole ($z'=0.5$) with an inlet $pO_2=50$ mm Hg, $R_{NO,max}=$ 300 μM/s and 150 μM/s, an arteriole *hct* consisting of 22.5% with HBOCs at the necessary concentration in order to bring the total heme concentration up to 9.6 mM (equivalent to RBCs at 45% *hct*), and without Mb in the tissue space. There are two controls in each subplot figure: the black line represents only RBCs at 22.5% *hct* (or 50% blood loss) and the dashed black line represents only RBCs at a normal *hct* of 45% (no blood loss). The HBOC mass concentration varies due to the molecular weight of the particular HBOC, however the total molar heme concentration of RBCs plus HBOCs is kept constant and equal to the average molar heme concentration of RBCs at 45% *hct*, which is 9.6 mM.

At an inlet $pO_2=50$ mm Hg, the HBOC buffers the pO_2 across the entire arteriole, as seen in Fig. 3A and C. The pO_2 profile with HBOCs remains close to that of plain RBCs, regardless of the HBOC's P_{50}. Conversely, the [NO] decreases by about half upon transfusion of HBOC, Fig. 3B and D. Although each HBOC has a different NO association rate constant, the maxima of the NO profiles were below 100 nM for each HBOC with the exception of rHb3011. The peak for the rHb 3011 [NO] curve, at a maximum $R_{NO,max}=300$ μM/s, is about 130 nM and 60 nM for $R_{NO,max}=150$ μM/s. The maximum centerline [NO] for the remaining HBOCs at $R_{NO,max}=300$ μM/s are 87.6, 85.8, 85.2, and 85.0 for MP4, PolyBvHb, rHb 1.1, and wt Hb, respectively.

Fig. 4, represents the same situation in Fig. 3 but includes Mb in the tissue space. The profiles at an inlet pO_2 of 10 and 5 mm Hg with and without Mb in the tissue space are included in the Supplemental data section (Figs. S1–4). Mb appears to have little effect on the dissolved pO_2 profile, Fig. 4A and C, since the profiles are close to that of plain RBCs. The presence of Mb in the tissue space greatly influences the shape of the [NO] profile, Fig. 4B and D, as there is almost no NO left in

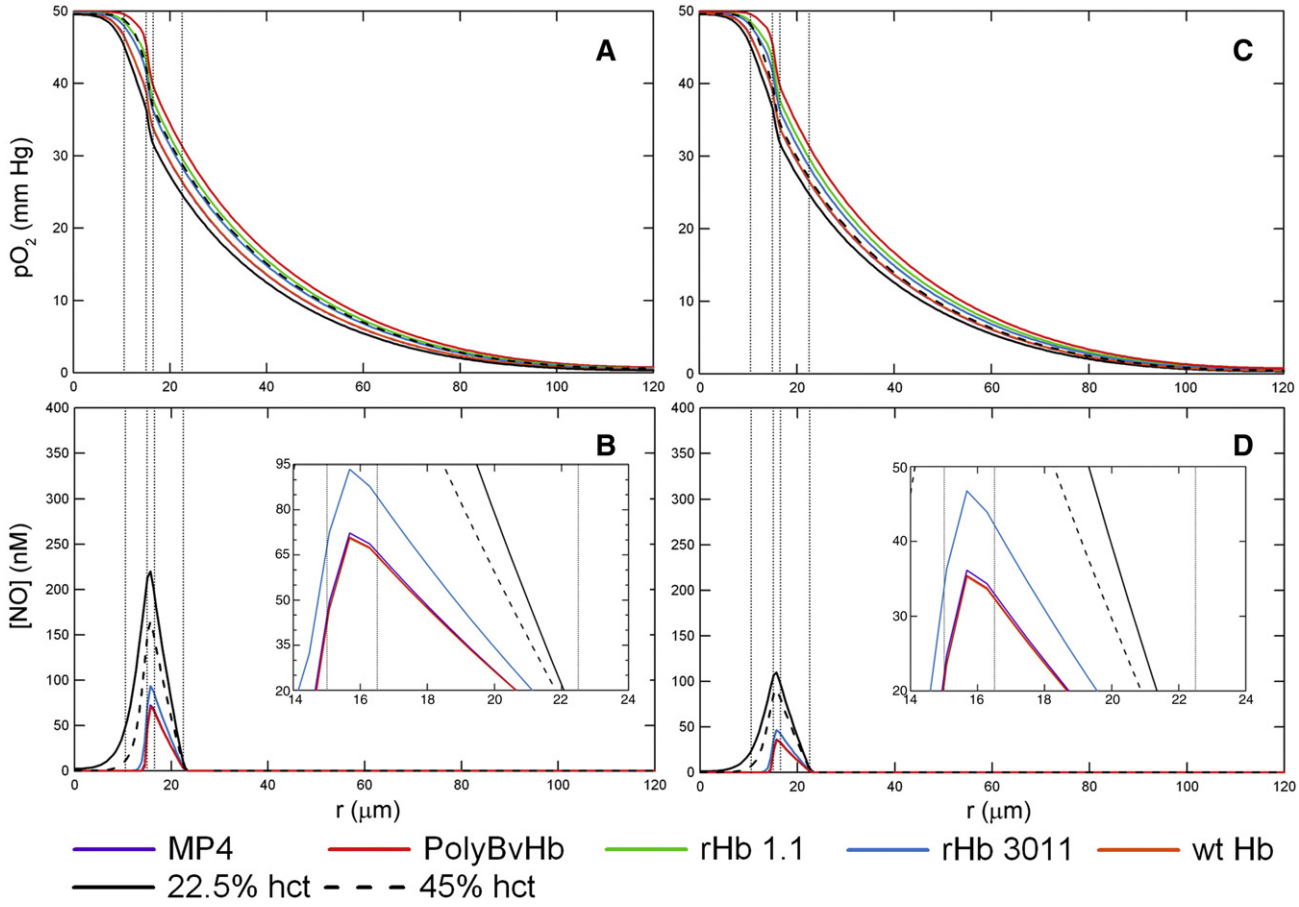

Fig. 4. O_2 tension profiles are shown at a *hct* of 22.5%, inlet $pO_2=50$ mm Hg with Mb in the tissue space at A) $R_{NO,max}=300$ μM/s and C) $R_{NO,max}=150$ μM/s. The corresponding [NO] profiles are shown at B) $R_{NO,max}=300$ μM/s and D) $R_{NO,max}=150$ μM/s. Transfusion of HBOCs replaced the lost RBC heme concentration to 22.5% *hct* (50% blood loss). The vertical lines represent the interface between the RBC-rich core region, RBC-depleted plasma layer and glyocalyx, endothelial vessel wall, interstitial space and smooth muscle cells, and tissue space.

the tissue space and the magnitude of the [NO] peaks are much less compared to when Mb is absent in the tissue space. Similar to simulations without Mb in the tissue space, the addition of HBOC decreases the [NO] in the endothelial vessel wall to about half of that without HBOCs. Of the HBOCs studied, rHb 3011 leaves the most NO in the whole arteriole-tissue region. If Mb is present, the [NO] peak with rHb 3011 is about 93.5 nM for $R_{NO,max} = 300$ μM/s and 47 nM for $R_{NO,max} = 150$ μM/s. The maximum centerline [NO] for the remaining HBOCs at $R_{NO,max} = 300$ μM/s are 72.3, 70.9, 70.5, and 70.5 nM for MP4, PolyBvHb, rHb 1.1, and wt Hb, respectively.

Low inlet pO_2 simulations exhibit similar pO_2 profile trends at an inlet $pO_2 = 50$ mm Hg. However, there is a noticeable, although slight, increase in the pO_2 profile of HBOCs mixed with 22.5% *hct* RBCs (solid black line) compared to RBCs at 45% *hct* (dashed black line) without HBOCs. This can be attributed to the HBOCs increased O_2 carrying capacity and higher heme concentration that is closer to the endothelial vessel wall. It is also evident in Figs. 3 and 4 that the pO_2 in the cell-free plasma layer is increased in the presence of HBOCs. Since HBOCs are smaller in size and can get closer to the arteriole wall compared to RBCs, they can significantly increase the local O_2 concentration in the cell-free plasma region.

The [NO] decreases with decreased O_2 availability (inlet pO_2) as its production is dependent on the O_2 tension (compare Figs. 3 and 4 to S1–4). Also, there is a sharp drop in the [NO] profile when Mb is present in the tissue space as it irreversibly binds NO (Figs. 3B and D versus 4B and D). Again, rHb 3011 yields the greatest amount of NO remaining in the arteriole space both with and without Mb in the tissue space. At $R_{NO,max} = 300$ μM/s and without Mb, the [NO] peak was 56 nM, and 28 nM when $R_{NO,max} = 150$ μM/se. If Mb is present in the tissue space, the [NO] peak for rHb 3011 drops to 44 nM when $R_{NO,max} = 300$ μM/s and 23 nM at $R_{NO,max} = 150$ μM/s.

Not only does the presence/absence of Mb in the tissue space control the magnitude of the [NO] profile, it also alters the entire shape of the [NO] profile. Without Mb in the tissue space, the [NO] will slowly decrease as it gets farther away from its endothelial wall source. In the presence of Mb in the tissue space, NO is quickly consumed and the [NO] drops steeply to zero at the inner edge of the tissue space.

Fig. 5 shows how the pO_2 and [NO] is affected as a function of *hct* at $R_{NO,max} = 300$ μM/s. There are two important points to consider about these figures. First, to be able to compare just the change in *hct*, the molar concentration of HBOC heme groups had to be set to the same value for every *hct* at ~4.8 mM heme. Although this may not reflect HBOC concentrations previously used *in vivo*, these values were chosen to make the total heme concentration constant between every HBOC and RBC solution in order to permit comparisons between the results of each mixture that was simulated. The total amount of heme groups will vary between different *hct*s as the RBC heme changes. Secondly, the vertical lines that designate the core region are spaced for 22.5% *hct* to be consistent with all previous figures. In reality, the simulations accounted for the core region's radial increase as the RBC *hct* increases. Again, there is very little change in the pO_2 as the *hct* increases. Close inspection shows all pO_2 profiles are closely packed together at 45% *hct* versus 22.5% near the exiting corner of the arteriole at $z = L_c$ and $r = R_c$. Also, the pO_2 profile for normal RBCs at 45% *hct* (black line) has a more step-like drop in pO_2 at the outskirt of the core region (i.e. r close to r_1) as opposed to the gradual decrease in pO_2 found with lower *hct*s. The pO_2 in the tissue region is about the same for all conditions studied, but is slightly elevated upon transfusion of HBOCs.

The [NO] decreases upon increasing the RBC concentration (Fig. 5-B, D, and F). The maximum [NO] at a 22.5% *hct* is 364 nM, 293 nM at 35% *hct*, and decreases to 234 nM at a normal *hct* of 45% without Mb in the tissue space. However, there is little distinguishable difference between *hct*s when HBOCs are transfused into the lumen. The supplemental data contains figures for the [NO] profiles of each HBOC (without Mb, Fig. S5, and with Mb, Fig. S6). The decrease in [NO] with increasing *hct* is noticeable, but the three *hct* curves for each HBOC are very similar to each other. rHb 3011 still leaves the greatest amount of NO in the vessel wall and there is some small variation between the *hct*s studied. With ~4.8 mM of rHb 3011 heme, the maximum [NO] is 116 nM at 22.5% *hct*, 114 nM at 35% *hct* and 112 nM at 45% *hct*.

When Mb is present in the tissue space, as shown in Fig. 6, the same trend exists between the maximum [NO] and the RBC *hct*, but the general shape of the curve is different. Also, the value of the

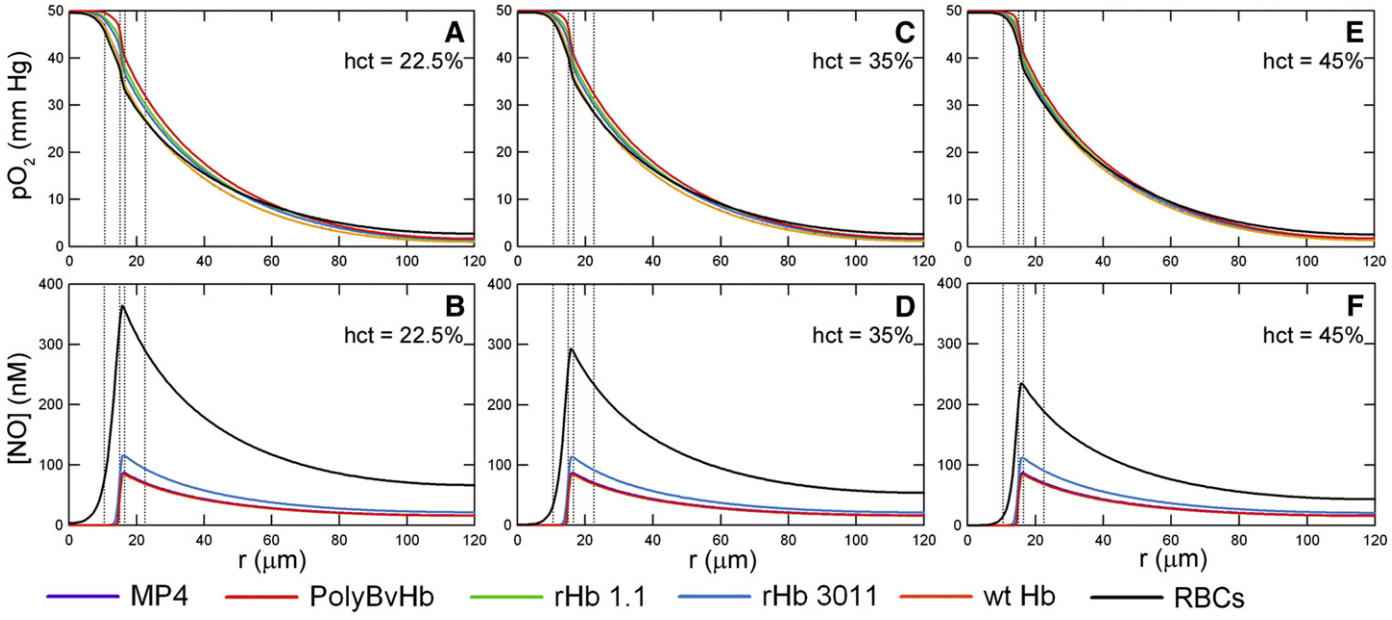

Fig. 5. O_2 tension and [NO] profiles at an inlet pO_2 of 50 mm Hg, $R_{NO,max} = 300$ μM/s, and [HBOC] = 9.6 mM heme at each simulated *hct* without Mb in the tissue space. A) pO_2 and B) [NO] profiles with 50% blood loss, i.e. 22.5% *hct*. C) pO_2 and D) [NO] profiles with 25% blood loss, i.e. 35% *hct*. E) pO_2 and F) [NO] profiles with no blood loss, i.e. 45% *hct*. The vertical lines represent the interface between the RBC-rich core region, RBC-depleted plasma layer and glyocalyx, endothelial vessel wall, interstitial space and smooth muscle cells, and tissue space.

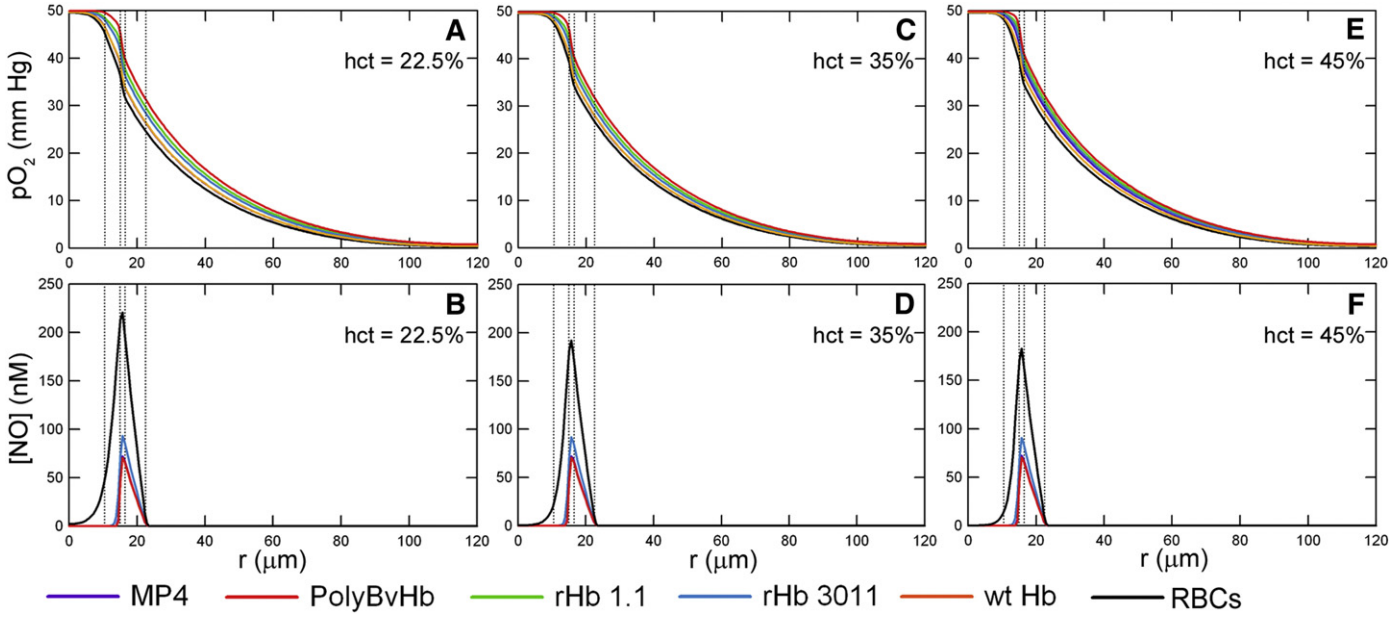

Fig. 6. O_2 tension and [NO] profiles at an inlet pO_2 of 50 mm Hg, $R_{NO,max} = 300$ μM/s, and 9.6 mM heme at each simulated *hct* with Mb in the tissue space. A) pO_2 and B) [NO] profiles with 50% blood loss, i.e. 22.5% *hct*. C) pO_2 and D) [NO] profiles with 25% blood loss, i.e. 35% *hct*. E) pO_2 and F) [NO] profiles with no blood loss, i.e. 45% *hct*. The vertical lines represent the interface between the RBC-rich core region, RBC-depleted plasma layer and glyocalyx, endothelial vessel wall, interstitial space and smooth muscle cells, and tissue space.

maximum [NO] is over 100 nM lower than without Mb in the tissue space. With just RBCs in the lumen of the arteriole, the maximum [NO] is 220 nM at 22.5% *hct*, 192 nM at 35% *hct* and 183 at 45% *hct*. HBOCs transfused in the lumen further decreases the total [NO] that is available in the arteriole. Transfusion of rHb 3011 leaves the greatest amount of NO remaining at 94 nM at 22.5% *hct*, 92 nM at 35% *hct* and 91 nM at 45% *hct*.

In general, the [NO] in the lumen and smooth muscle region is depleted by two factors. First, the NO concentration decreases when the total heme concentration is increased by either supplementation of HBOCs or RBCs. Secondly, there is naturally less NO available at lower NO production rates in the blood vessel wall.

2.2. O_2 transfer rate

Since it is important for HBOCs to deliver O_2 to the surrounding tissue space, this study also calculated the O_2 transfer rate. The O_2 transfer rate (k_o) is the flux of O_2 (in μM/s) across the G–E boundary per mm Hg of dissolved O_2 in the arteriole lumen. Fig. 7 displays the O_2 transfer rate versus the average arteriole pO_2 at $R_{NO,max} = 300$ μM/s and 22.5% *hct* for each HBOC at three different concentrations without Mb in the tissue space. The actual k_o values for tissues with Mb in the tissue space are slightly higher than tissues without Mb indicating a slight increase in O_2 transport with Mb present in the tissue space. For simulations with only RBCs in the lumen, the increase in k_o with Mb is noticeable even in this representation. When the HBOC k_o curves with and without Mb in the tissue space, are plotted on the same axis, the difference in k_o is undetectable in this representation and was therefore excluded in the discussion. Additional k_o plots show the data from simulations without Mb in the tissue space for simplicity, since this study primarily focuses on the effect of HBOCs on O_2 and NO tension. The supplemental data section has similar figures for *hcts* of 35% (Fig. S7) and 45% (Fig. S8).

It is evident that k_o increases upon transfusion of HBOCs or RBCs after blood loss. Therefore, more O_2 is transported across the blood vessel wall upon transfusion of HBOCs to 22.5% *hct* RBCs. It is easy to see that k_o's dependence on $\langle pO_2 \rangle_{arteriole}$ is influenced by the HBOC's P_{50} as there is a peak in the k_o curve close to the HBOC's P_{50}. Since the

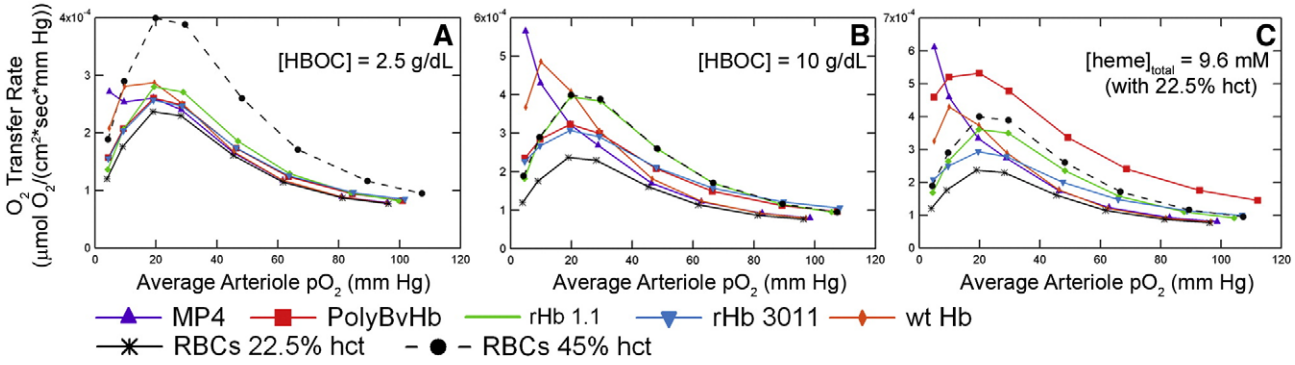

Fig. 7. O_2 transport rate across the arteriole wall at $R_{NO,max} = 300$ μM/s and 22.5% *hct* (50% blood loss). A) Simulations with 2.5 g/dL of HBOC without Mb in the tissue space. B) Simulations with 10 g/dL of HBOC without Mb in the tissue space. C) Simulations with 9.6 mM HBOC heme without Mb in the tissue space. At 22.5% *hct*, 9.6 mM of exogenous heme groups are needed to equal the total amount of heme groups found in normal RBCs at 45% *hct*. This equates to 11.36 g/dL of MP4, 7.65 g/dL of rHb 1.1, 7.65 g/dL of wt Hb, 7.65 g/dL of rHb 3011, and 40.2 g/dL of PolyBvHb. The vertical lines represent the interface between the RBC-rich core region, RBC-depleted plasma layer and glyocalyx, endothelial vessel wall, interstitial space and smooth muscle cells, and tissue space.

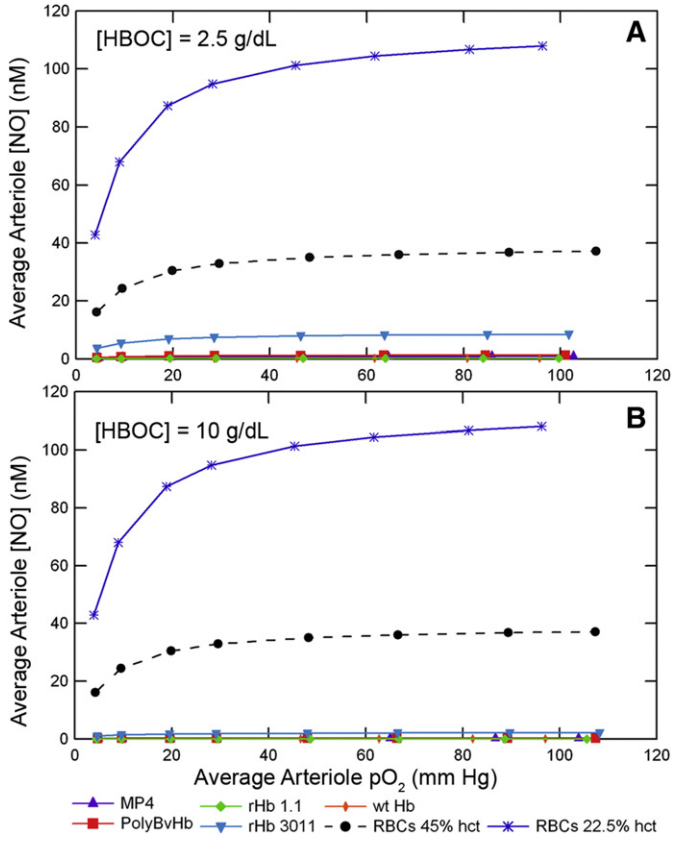

Fig. 8. Average arteriole [NO] versus the average arteriole pO_2 with A) 2.5 g/dL and B) 10 g/dL HBOC supplementation of RBCs at 22.5% *hct* and $R_{NO,max} = 300$ μM/s. The blue line represents the average arteriole [NO] with only RBCs at 22.5% *hct*. The black dashed line is a control of normal physiological RBCs at 45% *hct*.

release of O_2 is dictated by the slope of the O_2-HBOC equilibrium curve (dY/dpO_2), the HBOC/RBC will release most of its O_2 cargo when the slope is steepest, which is at the P_{50}. The recombinant Hbs (rHb 1.1 and rHb 3011) possess P_{50}s that are slightly higher than RBCs, but their k_o curves follow the same general shape of the pure RBC curve with a maximum k_o at $<pO_2>_{arteriole} \approx 20$ mm Hg. The recombinant Hbs naturally increase the k_o over RBCs at 22.5% *hct*, but at a $[heme]_{total} = 9.6$ mM their k_o curve was still lower in magnitude compared to RBCs at 45% *hct* (same $[heme]_{total}$ of only RBCs). These Hbs do show an increase in O_2 transport, but not equaling that of normal blood. Wild type Hb, with a lower P_{50} of 12.4 mm Hg, reaches a maximum pO_2 at ≈10 mm Hg with increasing concentrations of wt Hb. At 2.5 g/dL of wt Hb, the k_o curve still has maxima close to the RBC maxima at 22.5% *hct* and $<pO_2>_{arteriole} \approx 20$ mm Hg, since RBCs are still responsible for most of the O_2 transport.

MP4 has the most interesting k_o curves due to its low P_{50} (5.3 mm Hg), shown in the Fig. S9. At the highest concentrations of MP4, k_o experiences a sharp increase as the $<pO_2>_{arteriole}$ decreases. At lower concentrations corresponding to 2.5 g/dL and 5 g/dL of MP4, two peaks can be seen, one at a higher pO_2 close to the P_{50} of RBCs and another at a lower pO_2 near the P_{50} of MP4. This case reveals the separate effects of both RBCs and MP4 on O_2 transport.

In general, transfusion of any HBOC will improve the k_o across the blood vessel wall at 22.5% RBC *hct*. However, not all HBOCs have larger values of k_o when compared to the O_2 transport ability of RBCs at physiological *hct* (45%). HBOCs with a lower P_{50}, MP4 and wt Hb, require lower concentrations compared to other HBOCs to meet or surpass the k_o of 45% *hct* RBCs at low values of $<pO_2>_{arteriole}$.

There is also little change in the overall O_2 transfer rate due to differences in NO production rates as shown Fig. S10, supplemental data section. Although the maximum NO production rate is fairly large, the volume in which NO is produced is comparatively small and has limited effect on the total O_2 tension. The maximum [NO] in the vessel wall is less than 400 nM which requires less than ~0.3 mm Hg O_2 to synthesize. Even under extreme hypoxic conditions ($pO_{2,in} =$ 5 mm Hg), this is a very small fraction of the total pO_2 available in the arteriole.

2.3. Average arteriole NO concentration

One primary goal of this study was to determine the extent of a particular HBOC's ability to scavenge NO. The average arteriole [NO], $<NO>_{arteriole}$, represents the volume averaged [NO] across the cell-rich arteriole core and the cell-depleted plasma layer. Increasing the concentration of any HBOC elicited a concomitant decrease in the $<NO>_{arteriole}$ by as much as two orders of magnitude as seen in Fig. 8. Fig. 8 displays the $<NO>_{arteriole}$ at 22.5% *hct* and $R_{NO,max} = 300$ μM/s

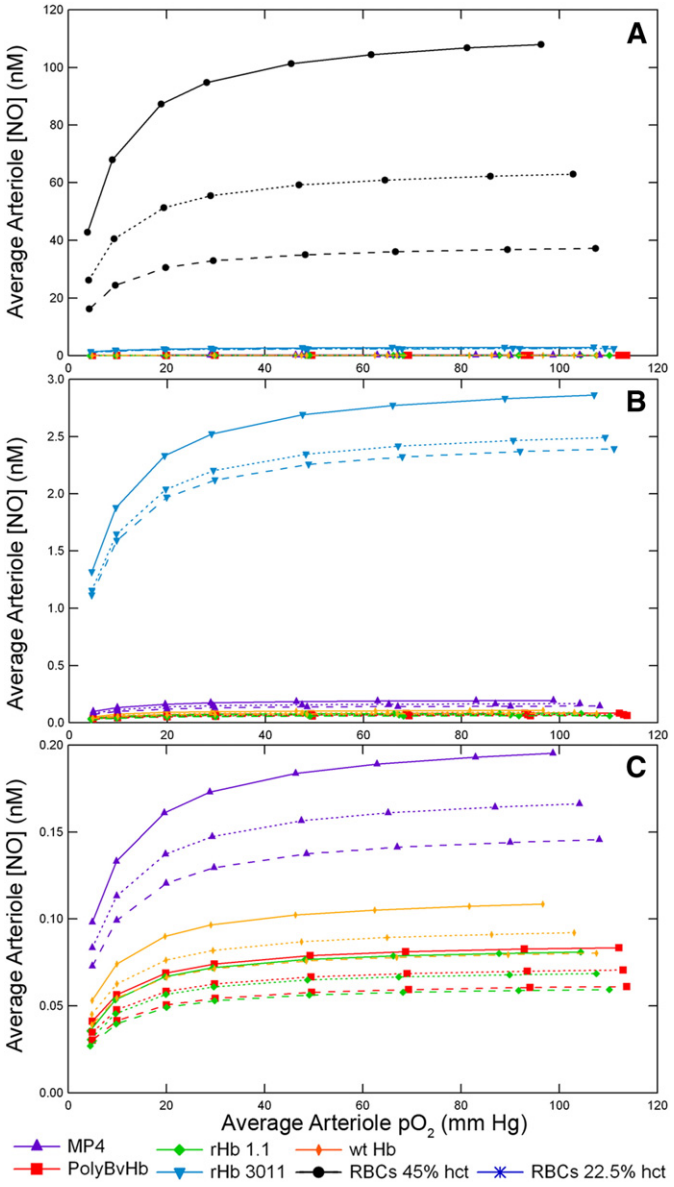

Fig. 9. Average arteriole [NO] versus the average arteriole pO_2 at various *hcts* with 9.6 mM HBOC and $R_{NO,max} = 300$ μM/s. The solid line is at a RBC *hct* of 22.5%, dotted line is at a RBC *hct* of 35%, and the dashed line is at a RBC *hct* of 45%. The three figures represent the same data set with sequential magnification of the Average Arteriole [NO] axis. A) Normal range of arteriole [NO] from 0 to 120 nM NO, B) Magnified to range from 0 to 3 nM NO, and C) Magnified to range from 0 to 0.2 nM of NO.

without Mb in the tissue space at two concentrations of HBOCs. Sequential magnifications of Fig. S8C in Fig. S11, show quite clearly that each HBOC scavenges different amounts of NO. Mb further scavenges NO in the arteriole (dotted line). This representation again shows that of all the HBOCs studied, rHb 3011 scavenged the least amount of NO. After rHb 3011, MP4 at the same heme concentration left the next greatest amount of NO remaining in the arteriole, followed by wt Hb, PolyBvHb, and rHb 1.1, respectively.

The next comparison, in Fig. 9, is between different *hct*s of RBCs. Even though the NO association rate constant between the heme contained inside RBCs is much slower compared with acellular HBOCs, increasing the arteriole *hct* decreases the [NO]. The increase in *hct* not only increases the total amount of heme groups, but also increases the concentration of heme in the cell-depleted plasma layer that is closer to the NO producing blood vessel wall. At each *hct*, rHb 3011 still scavenged the least amount of NO. As can be discerned from the magnifications in Fig. 9B and C, after rHb3011, MP4 left the next greatest amount of NO in the arteriole followed by wt Hb, PolyBvHb, and rHb 1.1.

The final comparison evaluates the effect of the different rates of NO production inside the blood vessel wall, $R_{NO,max}$ in Fig. S12. As would be expected, at the lowest rate of NO production, there is less overall NO in the arteriole. At $<pO_2>_{arteriole}$ above 40–50 mm Hg, the pO_2 is much greater than K_{m,O_2-NO} for NO formation, which causes the $<NO>_{arteriole}$ to plateau and at this point the [NO] does not increase much with further increases in pO_2. Again these data show the same NO trend with rHb 3011 leaving the largest amount of NO in the arteriole, followed by MP4, wt Hb, PolyBvHb, and rHb1.1, respectively.

3. Discussion

HBOCs have the potential to be very useful in clinical settings that involve replacing lost RBCs. However, clinical trials have noted an increase in MAP that has been attributed to vasoconstriction upon HBOC administration [1–4]. While there are many different types of HBOCs that have a variety of physical properties that can elicit vasoactivity, this mathematical model focuses on the effect of transfused HBOCs on the O_2 and NO concentration profiles throughout the arteriole and tissue region in the presence of RBCs in the lumen and Mb in the tissue space.

3.1. Effect of RBC hematocrit

Although the NO consumption rate of RBCs is relatively slow compared to acellular Hb and HBOCs, the [NO] profile is affected by the RBC *hct* as can be seen by comparing the solid black lines in Fig. 5B, C, and F or Fig. 6B, D, and F. As the *hct* increases, the [NO] profile decreases, since there are more RBCs available to consume NO. Additionally at higher *hct*s, the size of the core cell-rich region increases and therefore the RBCs are closer to the NO producing endothelial cells in the blood vessel wall. Therefore, NO has less distance to diffuse, before it is consumed by RBC heme groups.

The change in RBC *hct* has a small effect on the pO_2 profile by remaining approximately the same for all *hct*s studied. One noticeable difference is the pO_2 value close to the endothelial vessel wall. At an increased *hct*, the RBCs are closer to the wall and increase the local pO_2 value in that region.

3.2. HBOC influence on pO_2 and NO profiles

In the case of blood loss, the [NO] profile will increase in magnitude as the available RBCs concentration decreases, however transfusion of more RBCs or HBOCs will be necessary to maintain oxygen transport at post blood loss levels. Transfusion of either RBCs or HBOCs will affect the [NO] profile. The [HBOC] distribution in the lumen will permit the HBOCs to be closer to the NO production source (E) and thus decrease the distance necessary for NO to diffuse before it is scavenged by HBOCs in the plasma layer. The distribution of HBOCs in the lumen, plus the HBOC's increased affinity for NO, will facilitate the NO arteriole concentration to drop nearly to zero in the lumen.

The [NO] profile remains approximately constant with an equal concentration of HBOCs at different RBC *hct*s (Fig. 5B, D, and F). The overall NO consumption rate is dependent on the total amount of heme available, and is also dependent on the consumption rate constant of NO by RBCs and HBOCs. Although the RBC-heme concentration changes with *hct*, its rate constant with NO (k_{NO}) is several orders of magnitude slower compared to acellular HBOCs. Therefore HBOCs at a constant concentration, will dominate NO consumption and thus changes in RBC *hct* will not influence the [NO] profile.

On the other hand, the pO_2 profiles for transfused HBOCs were slightly increased compared to simulations with only RBCs, with the largest difference occurring at the lowest inlet pO_2 of 5 mm Hg (compare Figs. 3 and 4 to Figs. S3 and S4). These pO_2 profiles show that transfusion of HBOCs increased the pO_2 closer to the endothelial vessel wall. Since HBOCs are able to distribute more evenly across the whole arteriole space, they provide a blunted pO_2 profile compared to RBCs alone. The increase in *hct* also provided the same blunted pO_2 profile as more RBCs were closer to the endothelial wall.

3.3. Red muscle tissue (with Mb) versus normal tissue (without Mb)

Since it can be assumed that HBOCs will be evenly distributed throughout the entire systemic circulation, they will be transported through arterioles in red muscle tissue and normal (non-muscle) tissue. This can elicit significant differences in [NO] profiles, since Mb in red muscle tissue possess heme groups that can scavenge NO. The presence of Mb in the tissue space lowers the [NO] even further throughout the entire arteriole tissue region. More specifically, Mb in the tissue space drops the peak [NO] nearly in half and the tissue space [NO] to zero as shown in Figs. 4, 6, S2, S4, and S6. This drastic drop in tissue [NO] with Mb present in the tissue space is attributed to the ability of Mb's heme group to scavenge NO. According to these simulations, most of the smooth muscle cells would be exposed to NO concentrations below the calculated value of 23 nM NO necessary for half-maximal sGC activation. This result could be the cause for the observed *in vivo* increases in MAP upon transfusion of acellular HBOCs [1,4]. This mathematical model assumed that there is no reverse reaction rate with NO and Mb (NO dissociation from Mb), since this reaction is much slower than the forward reaction. Therefore, even if the reverse reaction was considered in the current model, it would not increase the [NO] profile appreciably and the [NO] profile would still be much lower than simulations that omit Mb in the tissue space.

By comparing all radial [NO] curves with $R_{NO,max} = 300$ μM/s without Mb in the tissue space, the [NO] appears to remain above the amount needed to promote vasorelaxation in the smooth muscle region, Figs. 3B, 5, S1, S3, and S5. However, once Mb is included in the tissue space, the [NO] drops to zero in the lumen of the arteriole and tissue space (Figs. 4B, 6, S2, S4, and S6). In the smooth muscle region, the [NO] in the presence of HBOCs ranges from just below 100 nM to 0 nM and approximately half of the smooth muscle cells should experience less than Condorelli's 50% sGC activation. The combination of both HBOCs in the lumen and Mb in the tissue space scavenging NO could be a significant cause for the vasoconstrictive effect, due to the low dissolved [NO] in the arteriole.

According to Condorelli's reported value of 23 nM NO for half-maximal sGC activation, it would seem than the scenarios presented in this model without Mb present in the tissue space should allow for some sGC activation [6]. However, experimental studies have found that these HBOCs do, in fact, increase the MAP. A review by Olson et al. reported studies that found rHb1.1 elicited an increase in MAP that was ten times stronger compared to rHb3011[4]. Tsai et al. also

observed MP4 and PolyBvHb to elicit an approximately equivalent increase in relative MAP [1]. A subsequent hamster window study preformed by Tsai et al. found a decrease in NO tissue concentration and an increase in MAP with transfusion of MP4 and PolyBvHb [35]. However, MP4 did not elicit the corresponding vasoconstriction. They attribute MP4's lack of vasoconstriction to its other unique physiological properties and may be due to the fact that MP4 substantially increases blood volume. Even with 50% sGC activation as implied by this study, more NO might be needed to achieve sufficient relaxation of the vessel walls. It is also possible that extravasation of HBOCs into the arteriole wall and surrounding layer of smooth muscle cells could scavenge even more NO and thus lower sGC activation even further.

3.4. Endothelial NO production rates

Since a range of NO production rates, $R_{NO,max}$, are cited in the literature and there are different opinions as to the magnitude of these values, this study evaluated two different NO production rates and compared the results to simulations with no NO production. These simulations had to balance NO's opposing effects on the pO_2 level in the tissue space. In fact, NO production is a drain on the local O_2 supply, because O_2 is required to produce NO in the endothelial wall. Alternatively, NO can increase the amount of dissolved O_2 that is made available to surrounding tissues, since it inhibits O_2 consumption by the tissues. A study by Lamkin–Kennard [36] observed that as $R_{NO,max}$ increased, the pO_2 in the tissue region increased due to NO inhibition of O_2 consumption. In this study, a slight increase in tissue pO_2 was observed, about 1–2 mm Hg at most, when HBOCs were absent in the lumen. However, transfusing HBOCs in the lumen decreased the tissue pO_2 with increasing $R_{NO,max}$ at the same total concentration of heme. It is possible that as more NO reacts with HBOCs, more O_2 will be required to create NO in the endothelial vessel wall, while less NO is available to inhibit O_2 consumption in the tissue space.

As shown in Fig. 3B, at a high rate of NO production (300 μM/s), the [NO] in the smooth muscle layer with rHb 3011 and 22.5% *hct* ranges from 100 nM to 130 nM. Although initial studies reported that sGC required ~250 nM of NO for vasorelaxation, later studies reported that 5–100 nM of NO is sufficient to activate sGC with a theoretical half-maximal activation of 23 nM NO [6,37]. Therefore, rHb 3011 should leave a sufficient amount of NO to activate sGC and should not elicit vasoconstriction. The other HBOCs reduce the NO concentration below 100 nM, while maintaining it above 50 nM. Although this should be enough to allow half-maximal sGC activation, there may not be enough activated sGC to prevent an increase in MAP due to vasoconstriction.

3.5. O_2 transport capability

While the primary purpose of this study was to investigate the changes in arteriolar [NO] upon transfusion of HBOCs, it is still just as important that HBOCs in the lumen allow sufficient delivery of O_2. In general, the pO_2 profile across the arteriole was not extensively influenced by the presence of NO or $R_{NO,max}$ as the [NO] are usually ~1000 times less than the O_2 concentration (in μM), as seen in Figs. 3–6, S1–S4. Other studies have also reported a small difference in pO_2 of about 1–2 mm Hg in the endothelial wall between $R_{NO,max} = 0$ and 300 μM/s [27,36].

In order to investigate O_2 transport of each HBOC, this study reported the pO_2 profiles and investigated the overall O_2 transfer rate (k_o, the flux of O_2 in μM across the endothelial vessel wall per mm Hg of dissolved O_2 available in the arteriole lumen) in Fig. 7. Generally, the O_2 transfer rate follows the trend described in previous studies [38,39] with maximal O_2 transfer occurring at a target pO_2 region close to each HBOC's respective P_{50} value. The P_{50} represents the point on the O_2 equilibrium curve with the greatest slope; thus a small change in the pO_2 in this region results in a large change in the fractional saturation of the HBOC, Fig. 1.

The k_o curves for MP4 are the most interesting due to MP4's low P_{50}. With lower concentrations of MP4, both MP4's and RBC's O_2 binding properties are reflected in the O_2 transport curve with two peaks seen on the curve. The first peak is just below the P_{50} of RBCs at $\langle pO_2 \rangle_{arteriole} \approx 20$ mm Hg, and the second peak is just below MP4's P_{50} of 5 mm Hg. When the total heme concentration is the same as that of RBCs at a 45% *hct*, MP4 (at 11.36 g/dL) dominates O_2 transport. But at lower than physiological heme concentrations, there is a more modest increase in MP4 facilitated O_2 transport. Since MP4 has such a low P_{50}, it will carry more O_2 at lower pO_2s than RBCs and will only release that extra O_2 at low pO_2s. This produces the two peaks in the k_o curve, where MP4 'holds on' to its O_2 while RBCs are at their maximum release rate of O_2 at moderate pO_2s. Then, once the RBCs have lost most of their bound O_2 at the lower pO_2, MP4 is in the region of its maximal O_2 release rate.

The k_o does not noticeably change with the inclusion of Mb in the tissue space. There was a very slight increase in the presence of Mb, but these differences were indistinguishable on the k_o versus average arteriole pO_2 curves and were therefore not shown. Since these simulations are at steady-state, Mb is nearly at its local saturation value and the remaining O_2 transported out of the arteriole space would be used mostly for tissue consumption.

At the lower [HBOC] with 22.5% *hct*, the k_o curves will be close to the curve for RBCs at 22.5% *hct* since not many HBOCs are available to increase O_2 transport. As the HBOC concentration is increased, there is a natural increase in the O_2 transfer rate as there are more HBOCs present to bind O_2. While some HBOCs surpass the k_o at a physiological heme concentration, such as PolyBvHb at all pO_2s and MP4 and wt Hb at lower pO_2s, the recombinant Hbs' k_o remain less than RBCs at 45% *hct*. Although the recombinant Hbs increase the O_2 transfer rate above RBCs at 22.5% *hct*, they are not able to increase the k_o to that of normal blood (RBCs at 45% *hct*).

3.6. Vasoconstriction due to autoregulation versus NO scavenging

Some initial theories attributed HBOC-induced vasoconstriction to an autoregulatory process that was initiated by an increase in O_2 transport across the blood vessel wall into the surrounding tissue space that was attributed to the presence of HBOCs in the systemic circulation [40,41]. Autoregulatory theory proposes that O_2 transport is increased (compared to RBCs) by the 'facilitated' diffusion of cell-free Hb due to the removal of diffusional barriers such as the RBC membrane and the unstirred plasma layer of RBCs. Natural physiological mechanisms controlling O_2 supply in the systemic circulation then sense the increase in O_2 transport from cell-free Hb and constrict the blood vessel in response to the increased O_2 supply [41]. While the circulatory system does have this response when too much O_2 is delivered to the blood vessel wall as explained by Cabrales et al., they also demonstrated that vasoconstriction and vasodilation is dependent on NO availability [42]. Furthermore, Cabrales et al. reported that the [NO], and subsequent vasoconstriction/vasodilation, is influenced by a NO scavenger. This leads to the suggestion of another physiological mechanism controlling arteriole dilation and contraction.

Studies by Válquez et al. and Martini et al. showed that moderately increasing the concentration of RBCs actually dilated the blood vessel due to the increased shear stress at the arteriole wall which triggered increased NO production [43,44]. These studies did show an increase in blood pressure once a certain *hct* was surpassed due to fact that the NO production rate reached a plateau and the vessel wall's inability to dilate any further. Furthermore, Válquez et al.'s study also used metRBCs in which all the Hb in the RBC was oxidized to metHb (thus unable to bind with O_2 or NO) in order to increase the *hct*. Transfusion of metRBCs caused the blood vessels to dilate, supporting the theory that one trigger for vessel dilation is NO production due to increased shear stress and not increased O_2 transport across the blood vessel wall.

Martini et al. also increased the RBC *hct* in knockout mice unable to produce endothelial derived NO. These mice had no change in blood

pressure with increased RBC *hct*. If the hypothesis underpinning autoregulatory theory was correct, then increasing the RBC *hct* should lead to a corresponding increase in O_2 delivery, which should cause the blood vessel to constrict in order to reduce the $[O_2]$ in the tissue space. Also, it should be independent of the endothelium's ability to produce NO and similar responses would have been observed in both wild type and knockout mice unable to produce endothelial derived NO.

The results presented in this modeling study support the NO scavenging hypothesis. First of all, there are only slight changes in the pO_2 profile (O_2 tension) upon transfusion of HBOCs throughout most of the arteriole, especially the smooth muscle region, at inlet pO_2s close to normal physiological conditions. This is in agreement with other O_2 and NO transport simulations that report tissue O_2 profiles not considerably changed upon transfusion of HBOCs into the systemic circulation at moderate inlet pO_2s [27]. Since the pO_2 is not considerably altered with transfused HBOCs, this discourages the idea that vasoconstriction is due solely to an increase in O_2 transport.

Secondly this study shows a substantial decrease in the amount of NO that is available to smooth muscle cells in presence of HBOCs with and without Mb in the tissue space. This drop in the [NO] profile is dependent on the HBOC's rate of NO consumption (not O_2 tension). Of the HBOCs discussed in this study, rHb3011 exhibited the slowest reaction rate with NO and consequently left the most NO available throughout the arteriole tissue region as shown in the [NO] profiles of Figs. 3 through 6 and in the average arteriole [NO] of Figs. 8 and 9. The general trend of NO availability in the arteriole, from greatest to least, was rHb3011, MP4, wt Hb, PolyBvHb, and rHb1.1. This mostly follows the same trend of increasing $k_{NO-HBOC}$ (Table 1) with the exception of PolyBvHb. PolyBvHb's increased molecular size and decreased diffusivity could cause it to be poorly mixed and have a greater concentration near the arteriole wall where it can readily consume NO. These results agree with investigations by Doherty et al. and Olson et al., reporting that the degree of vasoconstriction is dependent on the cell-free Hb/Mb's reaction rate with NO [3,4]. Their results combined with the results of this study further support the NO scavenging theory to explain the vasopressor effect observed with *in vivo* HBOC trials.

The results of this modeling study and previous experimental studies confirm that HBOCs scavenge NO. Transfusion of HBOCs elicit concomitant NO scavenging, which is the most probable reason that HBOCs have been found to elicit hypertension in *in vivo* experiments. Various strategies have been investigated to mitigate NO scavenging by supplementing the vasculature with NO, either by inhalation of NO or injection of nitrite into the systemic circulation. In the study by Yu et al., mice that inhaled 80 ppm NO before transfusion of tetrameric Hb did not elicit an increase in MAP [45]. However, if NO was inhaled during tetrameric Hb transfusion, much of the Hb was oxidized to metHb. The same group also injected mice with nitrite prior to Hb transfusion. Nitrite also prevented acellular Hb induced hypertension, but resulted in an increase in the metHb level of transfused Hb.

4. Conclusions

The mathematical model developed in this study can be used to predict the vasopressor response associated with HBOC transfusion in the systemic circulation. Administration of HBOCs can deliver sufficient O_2 to surrounding tissues, however all acellular HBOCs will concomitantly scavenge large amounts of NO from the vasculature, thus leaving less activated sGC and therefore unable to relax the blood vessels. Although HBOCs can increase O_2 delivery to surrounding tissues in the case of blood loss, they cannot attain the same O_2 transport capabilities of a similar amount of RBCs. Considering the recombinant Hbs studied, the k_o and local pO_2 at 22.5% *hct* did not reach the same values for RBCs at 45% *hct* (no blood loss) at equivalent heme concentrations. Therefore vasoconstriction is not necessarily triggered by an increase in O_2 transport, especially if O_2 transport is less in the presence of HBOCs versus normal blood. Hence, the next most probable cause of vasoconstriction would thus originate from NO scavenging, as this study illustrated to be the case, even with low concentrations of HBOCs in the systemic circulation.

Acknowledgments

This work was supported by the National Institutes of Health grants R01HL078840 and R01DK070862 to AFP.

Appendix A. Governing transport equations

O_2 is primarily transported in the arteriole lumen, CR and CF, by the convective flow of dissolved O_2, RBCs and HBOCs in the plasma. There it diffuses out of the arteriole lumen through the protein glycocalyx layer and into the vascular wall. In the vascular wall, some O_2 is consumed by endothelial cells to produce NO and it continues to diffuse into the smooth muscle and tissue regions where is it also consumed by those tissues. NO is only produced by the endothelial vessel wall (E) and diffuses out of the wall to the surrounding tissues (SM and TS) and arteriole lumen. It is consumed predominately in the smooth muscle region, by heme groups in the arteriole and tissue region (Hb and Mb), and some is also consumed in the tissue space. NO also inhibits O_2 consumption by the smooth muscle and tissue cells.

The governing equations for dissolved O_2, oxyHb saturation inside RBCs, oxyHBOC saturation, Mb saturation, and dissolved NO were derived from mass balances on each individual species to yield a system of coupled nonlinear partial differential equations. These equations take into account convective and diffusive transport, as well as the kinetics of O_2 and NO binding/release to/from Hb inside RBCs and HBOCs, and Mb. The kinetics describing O_2 binding/release to/from Hb inside RBCs or HBOCs were developed using a one-step kinetic approach as described by Popel [24]. By using this approach, only the dissociation rate constant (k_-) and a mathematical relationship that describes the O_2–RBC/HBOC/Mb equilibrium (Hill or Adair Equation) are necessary in order to calculate the rate of formation of O_2 [21,24,25]. Only the O_2–RBC equilibrium curve is described by the four parameter Adair equation. Whereas, the O_2–HBOC and O_2–Mb equilibrium curves are both described by the Hill equation, since values for the P_{50} (pO_2 at which the RBC/HBOC/Mb is half-saturated with O_2) and cooperativity coefficient were easily found in the literature for these O_2 carriers versus the corresponding Adair parameters. Back calculation of the Adair parameters from the Hill parameters is inaccurate without the raw O_2–HBOC equilibrium curve data. For this reason, we did not use the Adair equation to mathematically describe the O_2–HBOC equilibrium curve.

Table 2 lists all of the values used for the rate constants for each species, diffusivity values, maximum consumption rates, Michaelis–Menten parameters, core *hct*, maximum fluid velocity, and other model parameters that are included in the derivations detailed below.

O_2–Hb reaction kinetics

The total amount of Hb (Hb_{total}) consists of unbound Hb (Hb_{free}) and O_2 bound Hb (HbO_2) [21,24,25,46]. Hence, $[Hb_{total}] = [Hb_{free}] + [HbO_2]$ (for either RBCs or HBOCs). The fraction of the actual O_2 saturated Hb is given by Eq. (A1).

$$S = \frac{[HbO_2]}{[Hb_{total}]} \tag{A1}$$

Rearranging this expression yields Eq. (A2).

$$[HbO_2] = S \times [Hb_{total}] \text{ and } [Hb_{free}] = [Hb_{total}] \times (1 - S) \tag{A2}$$

Table 2
Physical and dimensional parameters of the simulated arteriole region.

Constants and model parameters			Description
Arteriole space			
$pO_{2,in}$	5, 10, 20, 30, 50, 70, 95, 115	mm Hg	Arteriole inlet O_2 tension
L_c	500	μm	Length of arteriole [27]
R_c	15	μm	Radius of arteriole [27]
U_{avg}	0.15	cm/s	Maximum velocity of arteriole flow [27]
$[Hb_{RBC}]$	34	g/dL	Total concentration of Hb inside a RBC
Hct	22.5%, 35%, 45%		Overall arteriole RBC hct
D_{O_2}	f([Hb]) [g/dL]	cm^2/s	Diffusivity of O_2 [21]
D_{Hb}	f([Hb]) [g/dL]	cm^2/s	Diffusivity of RBC Hb [21]
D_{NO}	0.000033	cm^2/s	Diffusivity of NO [27]
$[NO]^o$	0.01	μM	Characteristic NO concentration
A_1	2.59×10^{-3}	1/mm Hg	Adair constant for RBCs
A_2	1.77×10^{-3}	$1/mm\ Hg^2$	Adair constant for RBCs
A_3	1.86×10^{-11}	$1/mm\ Hg^3$	Adair constant for RBCs
A_4	1.39×10^{-6}	$1/mm\ Hg^4$	Adair constant for RBCs
RBC rich core			
α	1.34	μM/mm Hg	Solubility of O_2 in the arteriole core [27]
λ	0.7, 0.8, 0.9		RBC rich fraction of total core, dependent on hct [32]
R_1	10.5, 12, 13.5	μm	Radius of RBC rich core, dependent on hct
RBC depleted plasma region			
α	1.34		Solubility of O_2 in the plasma region [27]
R_2	14.5	μm	Outer radius of plasma region
r_2-r_1	4, 2.5, 1	μm	Thickness of plasma region
Glycocalyx			
R_c (r_3)	15	μm	Outer radius of glycocalyx
r_3-r_2	0.5	μm	Thickness of glycocalyx [27]
α	1.34	μM/mm Hg	O_2 solubility in glycocalyx [27]
D_{O_2}	0.000028	cm^2/s	Diffusivity of O_2 [27]
D_{NO}	0.000033	cm^2/s	Diffusivity of NO [27]
Endothelial vessel wall			
R_4	16	μm	Outer radius of vessel wall
r_4-r_3	1	μm	Thickness of vessel wall [27]
α	1.34	μM/mm Hg	O_2 solubility in vessel wall [27]
D_{O_2}	0.000028	cm^2/s	Diffusivity of O_2
D_{NO}	0.000033	cm^2/s	Diffusivity of NO [27]
$R_{NO,max}$	0, 150, 300	μM/s	Rate of NO production from O_2 [27]
K_{m,O_2-NO}	4.7	mm Hg	Rate constant for NO production from O_2 [27]
Interstitial region			
R_5	16.5	cm	Outer radius of interstitial region
r_5-r_4	0.5	μm	Thickness of interstitial region [9,23]
α	1.10	μM/mm Hg	O_2 solubility in interstitial region [21]
D_{O_2}	2.18×10^{-5}	cm^2/s	Diffusivity of O_2 [21]
D_{NO}	0.000033	cm^2/s	Diffusivity of NO [27]
Smooth muscle region			
R_6	22.5	μm	Outer radius of smooth muscle region
r_6-r_5	6	μm	Thickness of smooth muscle region [9,23]
α	1.34	μM/mm Hg	Solubility of O_2 in smooth muscle region [27]
D_{O_2}	0.000028	cm^2/s	Diffusivity of O_2 [27]
D_{NO}	0.000033	cm^2/s	Diffusivity of NO [27]
$Q_{max,sm}$	1	μM/s	O_2 consumption rate of smooth muscle cells [27]
K_m	1	mm Hg	Michaelis–Menten constant [27]
$k_{NO,sm}$	0.05	1/(μM s)	First order rate constant of NO consumption [9,23]
Tissue space			
R_7	120	μm	Outer radius of tissue [27]
r_7-r_6	97.5		

Table 2 (*continued*)

Constants and model parameters			Description
Tissue space			
α	1.52	μM/mm Hg	Solubility of O_2 in the tissue space [21]
D_{O_2}	2.41×10^{-5}	cm^2/s	Diffusivity of O_2 [21]
D_{NO}	0.000033	cm^2/s	Diffusivity of NO [27]
$Q_{max,tissue}$	20	μM/s	O_2 consumption rate of smooth muscle cells [27]
K_m	1	mm Hg	Michaelis–Menten constant [27]
$k_{NO,tissue}$	0.05	1/(μM s)	First order rate constant of NO consumption [9,23]
P_{50}, Mb	5.3	mm Hg	P_{50} of Mb in the tissue space [21]
D_{Mb}	6.00×10^{-7}	cm^2/s	Diffusivity of Mb in the tissue space [21]
k_{O2-Mb}	6.50×10^{1}	1/s	Dissociation rate constant of O_2 from Mb [21]
$[Mb]_{total}$	400.00	μM	Total concentration of Mb in the tissue space [21]
k_{NO-Mb}	43.00	1/(μM s)	Consumption of NO by Mb [9]

Although Hb has four gaseous ligand binding sites, a simple one-step reaction of one O_2 molecule binding to one heme group can be used to derive the rate of formation of O_2, which is derived from the following one-step chemical reaction, Eq. (A3).

$$O_2 + Hb_{free} \underset{k_-}{\overset{k}{\rightleftarrows}} HbO_2 \tag{A3}$$

The rate of oxyHb dissociation (or Hb or O_2 formation) is described by Eq. (A4).

$$R_{O_2} = k_-[HbO_2] - k[O_2][Hb_{free}] \tag{A4}$$

This equation and subsequent rate laws involving Hb treat Hb as one free heme group (one fourth of the total number of heme groups in the tetrameric Hb protein). The dissociation rate constant is denoted by k_-, while k denotes the association rate constant. At equilibrium, $S \rightarrow Y_e$. Therefore, the equilibrium fraction of O_2 saturated Hb, Eq. (A5), is described by the Adair or Hill equation [33,46]:

$$Y_e = \frac{[HbO_2]}{[Hb_{total}]} \tag{A5}$$

The rate of formation of Hb or O_2 is zero at equilibrium. Therefore, setting $R_{O_2} = 0$ (Eq. (A6)), and solving for k yields Eq. (A7).

$$k_-[HbO_2] = k[O_2][Hb_{free}] \tag{A6}$$

$$k = \frac{k_-[HbO_2]}{[O_2][Hb_{free}]} = \frac{k_- Y_e Hb_{total}}{[O_2]^* Hb_{total}^*(1 - Y_e)} \tag{A7}$$

At equilibrium, $S = Y_e$, thus $[HbO_2] = Y_e[Hb_{total}][Hb_{free}] = [Hb_{total}](1 - Y_e)$. Substituting $[O_2] = \alpha pO_2$, where α is the solubility of O_2 in the plasma and pO_2 is the O_2 tension in units of mm Hg, from Henry's Law into the previous expression and solving for k yields:

$$k = \frac{k_- Y_e}{\alpha^* pO_2^*(1 - Y_e)} \tag{A8}$$

Hence, we can write the rate of formation of O_2 in the form:

$$R_{O_2} = k_-[HbO_2]_{actual} - \frac{k_- Y_e}{\alpha^* pO_2^*(1 - Y_e)}[O_2][Hb_{free}] \tag{A9}$$

Where $[HbO_2]_{actual}$ is the actual concentration of HbO_2, which is determined from S and is distinct and different from the equilibrium concentration of HbO_2 calculated from Y_e. Hence, S is the actual local value of the saturation (not constrained at equilibrium) and becomes Eq. (A10).

$$S = \frac{[HbO_2]_{actual}}{[Hb_{total}]} \text{ and } [Hb_{free}] = [Hb_{total}](1 - S). \tag{A10}$$

So, we can again rewrite the rate of formation of O_2 in the form:

$$R_{O_2} = k_{-}{}^{*}S^{*}[Hb_{total}] - \frac{k_{-}Y_e}{\alpha^{*}pO_2{}^{*}(1 - Y_e)}\alpha^{*}pO_2{}^{*}[Hb_{total}]^{*}(1 - S) \tag{A11}$$

Hence, the rate of formation of O_2 is given by Eq. (A12).

$$R_{O_2} = k_{-}{}^{*}[Hb_{total}]^{*}\left[S - \left(\frac{Y_e}{(1 - Y_e)}\right)(1 - S)\right] \tag{A12}$$

For Hb inside RBCs, $S = S_{RBC}$, $Y_e = Y_{RBC,\,e}$, $[Hb_{total}] = [Hb_{RBC,\,total}]$ and $k_{-} = k_{RBC-}$. For HBOCs, $S = S_{HBOC}$, $Y = Y_{HBOC,e}$, $[Hb_{total}] = [HBOC_{total}]$ and $k_{-} = k_{HBOC-}$. Therefore, the rate of formation of O_2 from HbO_2 inside RBCs is given by Eq. (A13).

$$R_{O_2} = k_{RBC-}{}^{*}\left[Hb_{RBC,total}\right]^{*}\left[S_{RBC} - \left(\frac{Y_{RBC,e}}{\left(1 - Y_{RBC,e}\right)}\right)(1 - S_{RBC})\right] \tag{A13}$$

And the corresponding rate of O_2 formation from O_2 dissociating from HBOC–O_2 is Eq. (A14).

$$R_{O_2} = k_{HBOC\_}{}^{*}[HBOC_{total}]^{*}\left[S_{HBOC} - \left(\frac{Y_{HBOC,e}}{\left(1 - Y_{HBOC,e}\right)}\right)(1 - S_{HBOC})\right] \tag{A14}$$

In this case, R_{O_2} is the rate of formation of O_2 (or Hb, because one O_2 molecule dissociates from one HbO_2 molecule leaving one molecule of Hb remaining). The rate of formation of HbO_2 is given by: $R_{HbO_2} = -R_{O_2}$. For Hb inside RBCs the rate equation becomes Eq. (A15).

$$R_{O_2} = k_{HBOC\_}{}^{*}[HBOC_{total}]^{*}\left[S_{HBOC} - \left(\frac{Y_{HBOC,e}}{\left(1 - Y_{HBOC,e}\right)}\right)(1 - S_{HBOC})\right] \tag{A15}$$

For the case of HBOCs, the rate of formation of HBOC–O_2 is given by Eq. (A16).

$$R_{HBOC-O_2} = k_{HBOC\_}[HBOC_{total}]\left[\left(\frac{Y_{HBOC,e}}{\left(1 - Y_{HBOC,e}\right)}\right)(1 - S_{HBOC}) - S_{HBOC}\right] \tag{A16}$$

Arteriole space (Lumen)

In the arteriole lumen, RBCs are assumed to behave as a homogenous fluid with the RBC concentration varying as a function of the *hct*. A *hct* profile was used to describe the spatial distribution of RBCs. This profile assumes a constant concentration of RBCs in the RBC core region that linearly decreases outside the core region as described by Chen et al. [27], Eq. (C1), where H_c is the hematocrit in the core region, defined between $r = 0$ and $r = r_1$. H_c was calculated by assuming conservation of RBC mass in the arteriole and using a plug flow velocity profile and is described in more detail in Appendix C. The CF region is defined between r_1 and r_2. The velocity profile was also assumed to be constant (plug flow) in the RBC-rich core region and decreased linearly in the plasma layer according to Chen et al.'s description, Eq. (D3) in Appendix D [27].

O_2 transport occurs within the arteriole space via convection and diffusion through the plasma, and reacts with Hb inside RBCs and HBOCs. Since O_2 will bind to both Hb contained inside RBCs and HBOCs, the R_{O_2} for both HBOCs and RBC Hb must be included in the transport analysis. The general mass balance for the rate of formation of O_2 inside the arteriole RBC-rich core and cell-depleted plasma layer is given by Eq. (A17).

$$v_z\frac{\partial O_2}{\partial z} = D_{O_2}\left[\nabla^2 O_2\right] + R_{O_2,RBC} + R_{O_2,HBOC} \tag{A17}$$

Where v_z is the velocity profile in the axial direction, z is the axial length, D_{O_2} is the diffusivity of dissolved O_2, $R_{O_2,RBC}$ is the rate of formation of O_2 from HbO_2 inside RBCs and $R_{O_2,HBOC}$ is the rate of formation of O_2 from HBOC–O_2. By rewriting the O_2 mass balance in terms of O_2 tension (via application of Henry's law) and replacing the reaction terms with the corresponding rate law, the mass balance on O_2 becomes Eq. (A18).

$$\alpha v_z\frac{\partial pO_2}{\partial z} = \alpha D_{O_2}\left[\nabla^2 pO_2\right] + k_{RBC\_}{}^{*}\left[Hb_{RBC,total}\right]^{*}\left[S_{RBC} - \left(\frac{Y_{RBC,e}}{\left(1 - Y_{RBC,e}\right)}\right)(1 - S_{RBC})\right] + k_{HBOC\_}{}^{*}[HBOC_{total}]^{*}\left[S_{HBOC} - \left(\frac{Y_{HBOC,e}}{\left(1 - Y_{HBOC,e}\right)}\right)(1 - S_{HBOC})\right] \tag{A18}$$

The dependence of $[Hb_{RBC,total}]$ and $[HBOC_{total}]$ on the hematocrit (*hct*) and the radial position is described further in Appendix C.

A similar general mass balance for the rate of formation of HbO_2 is given by Eq. (A19).

$$v_z\frac{\partial [HbO_2]}{\partial z} = D_{Hb}\left[\nabla^2[HbO_2]\right] + R_{HbO_2} \tag{A19}$$

Where D_{Hb} is the diffusivity of Hb and R_{HbO_2} is the rate of formation of HbO_2.

By substituting $[HbO_2] = S_{RBC}{}^{*}[Hb_{RBC,total}]$ and the reaction rate term, the balance on HbO_2 inside RBCs becomes:

$$v_z\frac{\partial S_{RBC}}{\partial z} = D_{Hb}\left[\nabla^2 S_{RBC}\right] + k_{RBC\_}\left[\left(\frac{Y_{RBC,e}}{\left(1 - Y_{RBC,e}\right)}\right)(1 - S_{RBC}) - S_{RBC}\right] \tag{A20}$$

Similarly for HBOCs, the HBOC–O_2 balance becomes:

$$v_z\frac{\partial S_{HBOC}}{\partial z} = D_{HBOC}\left[\nabla^2 S_{HBOC}\right] + k_{HBOC\_}\left[\left(\frac{Y_{HBOC,e}}{\left(1 - Y_{HBOC,e}\right)}\right)(1 - S_{HBOC}) - S_{HBOC}\right] \tag{A21}$$

Where D_{HBOC} is the diffusivity of HBOC. The derivation of the diffusion coefficients for O_2 (D_{O_2}), Hb (D_{Hb}), and HBOCs (D_{HBOC}) is described in Appendix D.

The remaining mass balance, Eq. (A22), in the lumen describes NO transport.

$$v_z\frac{\partial [NO]}{\partial z} = D_{NO}\left[\nabla^2[NO]\right] - R_{NO} \tag{A22}$$

Where D_{NO} is the diffusivity of NO and R_{NO} is the rate of NO consumption by Hb inside RBCs and HBOCs in the lumen. The reactions between NO and Hb inside RBCs or HBOC, are respectively, described in Eqs. (A23a) and (A23b).

$$NO + Hb_{RBC,total} \xrightarrow{k_{NO-RBC}} Hb_{RBC,total} \cdot NO \tag{A23.a}$$

$$NO + HBOC_{total} \xrightarrow{k_{NO-HBOC}} HBOC \cdot NO \tag{A23.b}$$

By assuming that NO can bind to Hb/HBOC and HbO_2/HBOC-O_2 at the same rate, only one rate constant is utilized to describe this reaction. The reverse reaction is also ignored because NO will irreversibly oxidize the heme to yield NO_3^-. Hence, NO is consumed and the heme will no longer be able to bind with O_2. The rate of NO consumption, R_{NO}, is given by Eq. (A24) [9,13,23].

$$R_{NO} = k_{NO-RBC}[NO]\left[Hb_{RBC,total}\right] + k_{NO-HBOC}[NO][HBOC_{total}] \quad (A24)$$

Substituting this rate law into the NO mass balance yields Eq. (A25).

$$v_z\frac{\partial[NO]}{\partial z} = D_{NO}\left[\nabla^2[NO]\right] - k_{NO-RBC}[NO]\left[Hb_{RBC,total}\right] - k_{NO-HBOC}[NO][HBOC_{total}] \quad (A25)$$

Glycocalyx layer

The glycocalyx layer is a thin stagnant layer of proteins that line the inside of the arteriole wall. Since the glycocalyx is defined as a stagnant layer [27,34], it is also assumed there are no HBOCs in this region. Although, larger proteins, including HBOCs, have been found in the glycocalyx, extravasation of HBOCs through the glycocalyx and into the tissue space has been omitted from this model. Ideally an HBOCs will not extravasate, but will still scavenge NO from the arteriole. Therefore, there is no reaction with O_2 or NO in the glycocalyx layer. O_2 and NO simply diffuse through this layer and their transport is described by Eqs. (A26) and (A27), respectively.

$$0 = \alpha D_{O_2}\left[\nabla^2 pO_2\right] \quad (A26)$$

$$0 = D_{NO}\left[\nabla^2[NO]\right] \quad (A27)$$

Endothelial layer (or vessel wall)

After passing through the stagnant glycocalyx layer, O_2 and NO can diffuse through the vessel wall. In this region, O_2 is consumed by the endothelial cells to synthesize NO. The rate of formation of O_2, R_{O_2}, and NO, R_{NO}, is described by Michaelis–Menten kinetics and is given by Eq. (A28) [27,47].

$$R_{O_2} = -R_{NO,max}\frac{pO_2}{pO_2 + K_m} \quad R_{NO} = R_{NO,max}\frac{pO_2}{pO_2 + K_m} \quad (A28)$$

Where $R_{NO,max}$ is the maximum rate of NO formation from O_2 in the endothelium and K_m is the Michaelis–Menten constant.

O_2 transport in the wall is controlled by diffusion through this region and consumption by the endothelial cells to synthesize NO. Conversely, transport of NO is controlled by diffusion through this region and therefore its formation is dependent on the local O_2 concentration. O_2 and NO transport in the endothelial layer are described by the following equations:

$$0 = \alpha D_{O_2}\left[\nabla^2 pO_2\right] - R_{NO,max}\frac{pO_2}{pO_2 + K_m} \quad (A29)$$

$$0 = D_{NO}\left[\nabla^2[NO]\right] + R_{NO,max}\frac{pO_2}{pO_2 + K_m} \quad (A30)$$

Interstitial layer

O_2 and NO transport in the interstitial layer is similar to the glycocalyx layer with just gas diffusion through the region. The equations describing NO and O_2 become:

$$0 = \alpha D_{O_2}\left[\nabla^2 pO_2\right] \quad (A31)$$

$$0 = D_{NO}\left[\nabla^2[NO]\right] \quad (A32)$$

Smooth muscle layer

The smooth muscle layer surrounds the arteriole and is the region primarily responsible for consuming NO to control arteriole diameter. O_2 and NO diffuse though this region and both are consumed by the smooth muscle cells. The rate of O_2 consumption in the smooth muscle layer follows Michaelis–Menten kinetics, but it is inhibited by the presence of NO as shown in Eq. (A33) [27,47].

$$R_{O_2,tissue} = -Q_{max,sm}\frac{pO_2}{pO_2 + aK_{sm}} \quad (A33)$$

Where $Q_{max,sm}$ is the maximum rate of oxygen consumption by the smooth muscle cells, and aK_{sm} is the apparent Michaelis–Menten parameter after accounting for O_2 consumption inhibition and is defined by $aK_{sm} = K_{sm}\left(1 + \frac{[NO]}{27nM}\right)$ with K_{sm} as the Michaelis–Menten constant under NO-free conditions.

Therefore the O_2 transport equation becomes

$$0 = \alpha D_{O_2}\left[\nabla^2 pO_2\right] - Q_{max,sm}\frac{pO_2}{pO_2 + \left(K_{sm}\left(1 + \frac{[NO]}{27nM}\right)\right)} \quad (A34)$$

NO tissue consumption, Eq. (A35), is described with a simple first order reaction with a rate constant k_{NO-sm}:

$$R_{NO} = -k_{NO-sm}[NO] \quad (A35)$$

The resultant mass balance on NO in the smooth muscle layer becomes Eq. (A36).

$$0 = D_{NO}\left[\nabla^2[NO]\right] - k_{NO-sm}[NO] \quad (A36)$$

Tissue space

To simulate red muscle tissue, the heme-based protein myoglobin (Mb) was included in the tissue space [21]. For non-red muscle tissue simulations, the Mb terms were simply omitted. Mb binds with O_2 and yields an O_2-Mb equilibrium curve that can be represented by the Hill equation (Appendix D) with a cooperativity coefficient of 1 [46]. Since Mb has only one O_2 binding site, it cannot display cooperative O_2 binding. Similarly to Hb, S_{Mb} represents the actual fractional saturation of Mb, Eq. (A37), and $Y_{Mb,e}$ is the fractional saturation of Mb at equilibrium, Eq. (A38), which is mathematically described by the Hill equation (Appendix D).

$$S_{Mb} = \frac{[MbO_2]}{[Mb_{total}]} \quad (A37)$$

$$Y_{Mb,e} = \frac{[MbO_2]_{at\ equilibrium}}{[Mb_{total}]} \quad (A38)$$

The total amount of Mb available is the sum of free Mb and Mb bound to O_2, Eq. (A39).

$$[Mb_{total}] = [Mb_{free}] + [MbO_2] \text{ and } [Mb_{free}] = [Mb_{total}](1 - Y_{Mb}) \quad (A39)$$

The formation of MbO_2 from Mb_{free} and O_2 is described by the following chemical equation, Eq. (A40).

$$O_2 + Mb_{free} \underset{k_{Mb\_}}{\overset{k_{Mb}}{\rightleftarrows}} MbO_2 \quad (A40)$$

The rate of O_2 formation from MbO_2 dissociation is given by Eq. (A41).

$$R_{O_2,Mb} = k_{Mb-}[MbO_2] - k_{Mb}\left[Mb_{free}\right][O_2] \quad (A41)$$

By solving for k_{Mb} in a similar manner to Hb and substituting k_{Mb} into the rate equation yields:

$$R_{O_2,Mb} = k_{Mb-}[MbO_2] - \frac{k_{Mb-}}{\alpha \cdot pO_2}\frac{Y_{Mb,e}}{\left(1 - Y_{Mb,e}\right)}[Mb_{free}][O_2] \tag{A42}$$

Replacing $[O_2]$ with αpO_2 and $S_{Mb} = \frac{[MbO_2]_{actual}}{[Mb_{total}]}$ yields

$$R_{O_2,Mb} = k_{Mb-}[Mb_{total}]\left[S_{Mb} - \frac{Y_{Mb,e}}{\left(1 - Y_{Mb,e}\right)}(1 - S_{Mb})\right] \tag{A43}$$

O_2 transport throughout the tissue space is controlled by diffusion, reaction with Mb, and consumption by the cells in the tissue space. The rate of O_2 consumption in the tissue space follows Michaelis–Menten kinetics, but it is inhibited by the presence of NO as shown in Eq. (A44).

$$R_{O_2,tissue} = Q_{max}\frac{pO_2}{pO_2 + aK_m} \tag{A44}$$

Where Q_{max} is maximum rate of O_2 consumption by the tissues and $aK_m = K_m\left(1 + \frac{[NO]}{27nM}\right)$.

Therefore, the governing mass balance on O_2 in the tissue space becomes:

$$0 = \alpha D_{O_2}\left[\nabla^2 pO_2\right] + R_{O_2,Mb} - R_{O_2,tissue} \tag{A45}$$

Substituting the two rate laws into the above equation yields the overall equation, Eq. (A46), that describes O_2 transport in the tissue space:

$$0 = \alpha D_{O_2}\left[\nabla^2 pO_2\right] + k_{Mb-}[Mb_{total}]\left[S_{Mb} - \frac{Y_{Mb,e}}{\left(1 - Y_{Mb,e}\right)}(1 - S_{Mb})\right] - Q_{max}\frac{pO_2}{pO_2 + \left(K_m\left(1 + \frac{[NO]}{27nm}\right)\right)} \tag{A46}$$

NO is consumed by cells in the tissue and by the heme in Mb. Therefore, NO tissue consumption is described by the simple first order reaction, Eq. (A47).

$$R_{NO,tissue} = -k_{NO,tissue}[NO] \tag{A47}$$

Where $k_{NO,tissue}$ is the first order rate constant for this reaction.

NO binds irreversibly with the heme in Mb, similarly to its reaction with Hb, Eq. (A48).

$$NO + Mb_{total} \xrightarrow{kNO-Mb} Mb \cdot NO \tag{A48}$$

Again, this reaction assumes that NO can bind with Mb or MbO_2 at the same rate. Therefore, only one rate constant is utilized to describe the two reactions. The reverse reaction is neglected in our analysis, since NO will irreversibly oxidize the heme, as with Hb. Therefore, the heme will no longer be able to bind with O_2. The rate of NO consumption by Mb is thus given by Eq. (A49).

$$R_{NO-Mb} = k_{NO-Mb}[NO][Mb_{total}] \tag{A49}$$

Therefore, the total rate of NO consumption in the tissue space is the sum of these two reactions

$$R_{NO} = k_{NO,tissue}[NO] + k_{NO-Mb}[NO][Mb_{total}] \tag{A50}$$

The resultant mass balance on NO in the tissue space with both rate terms included becomes:

$$0 = D_{NO}\left[\nabla^2[NO]\right] - k_{NO,tissue}[NO] - k_{MbNO}[NO][Mb_{total}] \tag{A51}$$

The final species in the tissue space is the saturation of Mb with O_2, S_{Mb}. The rate of oxyMb formation, R_{MbO_2}, is equal and opposite of the rate of O_2 formation from MbO_2. Therefore, $R_{MbO_2} = R_{O_2,Mb}$.

Where, $R_{MbO_2} = k_{Mb-}[Mb_{total}]\left[\frac{Y_{Mb,e}}{(1 - Y_{Mb,e})}(1 - S_{Mb}) - S_{Mb}\right]$.

Therefore, the general mass balance for the fractional saturation of Mb becomes Eq. (A52).

$$0 = [Mb_{total}]D_{Mb}\left[\nabla^2 S_{Mb}\right] + k_{Mb-}[Mb_{total}]\left[\frac{Y_{Mb,e}}{\left(1 - Y_{Mb,e}\right)}(1 - S_{Mb}) - S_{Mb}\right] - k_{NO-Mb}[NO][Mb_{total}] \tag{A52}$$

Where D_{Mb} is the diffusivity of Mb. The total concentration of Mb can removed from the equation resulting in the final form of Eq. (A53).

$$0 = D_{Mb}\left[\nabla^2 S_{Mb}\right] + k_{Mb-}\left[\frac{Y_{Mb,e}}{\left(1 - Y_{Mb,e}\right)}(1 - S_{Mb}) - S_{Mb}\right] - k_{NO-Mb}[NO] \tag{A53}$$

Nondimensionalization

The governing transport equations were scaled with characteristic parameters to render the system of equations dimensionless. The radial dimension (r) was scaled to the arteriole radius, R_c, which includes the RBC core, cell-depleted layer, and glycocalyx protein layer, Eq. (A54.a). The total arteriole length, L_c, was used to scale the axial dimension (z), Eq. (A54.b).

$$r' = \frac{r}{R_c} \tag{A54.a}$$

$$z' = \frac{z}{L_c} \tag{A54.b}$$

To completely nondimensionalize the system of equations, characteristic values were needed for the pO_2, NO, and velocity profile, Eqs. (A55a), (A55b) and (A55c). Since the fractional saturation values are already dimensionless, they do not need to be scaled. The pO_2 was scaled with the P_{50} of RBCs in the lumen and the velocity was scaled to U_{avg} which was a defined model parameter. Since there is no 'obvious' scaling factor for NO concentration, $[NO]^o$, an arbitrary value of 100 nM was chosen.

$$pO_2' = \frac{pO_2}{P_{50}} \tag{A55.a}$$

$$v_z' = \frac{v_z}{U_{avg}} \tag{A55.b}$$

$$[NO]' = \frac{[NO]}{[NO]^o} \tag{A55.c}$$

Substituting the dimensionless variables into the arteriole space results in the following equations, Eqs. (A56)–(A59), describing O_2 and NO transport:

$$\frac{\alpha U_{avg} P_{50} v_z'}{L_c}\frac{\partial pO_2'}{\partial z'} = \alpha D_{O_2} P_{50}\left[\nabla'^2 pO_2'\right] + k_{RBC-}\left[Hb_{RBC,total}\right]\left[S_{RBC} - \left(\frac{Y_{RBC,e}}{\left(1 - Y_{RBC,e}\right)}\right)(1 - S_{RBC})\right] + k_{HBOC-}[HBOC_{total}]\left[S_{HBOC} - \left(\frac{Y_{HBOC,e}}{\left(1 - Y_{HBOC,e}\right)}\right)(1 - S_{HBOC})\right] \tag{A56}$$

$$\frac{U_{avg}}{L_c} v_z' \frac{\partial S_{RBC}}{\partial z'} = D_{Hb}\left[\nabla'^2 S_{RBC}\right] + k_{RBC-}\left[\left(\frac{Y_{RBC,e}}{\left(1-Y_{RBC,e}\right)}\right)(1-S_{RBC}) - S_{RBC}\right] \tag{A57}$$

$$\frac{U_{avg}}{L_c} v_z' \frac{\partial S_{HBOC}}{\partial z'} = D_{HBOC}\left[\nabla'^2 S_{HBOC}\right] + k_{HBOC-}\left[\left(\frac{Y_{HBOC,e}}{\left(1-Y_{HBOC,e}\right)}\right)(1-S_{HBOC}) - S_{HBOC}\right] \tag{A58}$$

$$\frac{U_{avg}[NO]^o}{L_c} v_z' \frac{\partial [NO]'}{\partial z'} = [NO]^o D_{NO}\left[\nabla'^2 [NO]'\right] - k_{NO-RBC}[NO]\left[Hb_{RBC,total}\right] - k_{NO-HBOC}[NO][HBOC_{total}] \tag{A59}$$

The resulting transport equations in the tissue space for O_2, NO and MbO_2, respectively, results in Eqs. (A60)–(A62).

$$0 = \alpha D_{O_2} P_{50}\left[\nabla'^2 pO_2'\right] + k_{Mb-}[Mb_{total}]\left[S_{Mb} - \frac{Y_{Mb,e}}{\left(1-Y_{Mb,e}\right)}(1-S_{Mb})\right] - Q_{max}\frac{pO_2}{pO_2 + \left(K_m\left(1+\frac{[NO]}{27nM}\right)\right)} \tag{A60}$$

$$0 = [NO]^o D_{NO}\left[\nabla'^2 [NO]'\right] - k_{NO,tissue}[NO]^2 - k_{NO-Mb}[NO][Mb_{total}](1-S_{Mb}) - k_{NO-MbO_2}[NO][Mb_{total}]S_{Mb} \tag{A61}$$

$$0 = D_{Mb}\left[\nabla'^2 S_{Mb}\right] + k_{Mb-}\left[\frac{Y_{Mb,e}}{\left(1-Y_{Mb,e}\right)}(1-S_{Mb}) - S_{Mb}\right] \tag{A62}$$

The dimensionless pO_2 and NO for the stagnant layers, glycocalyx and interstitial space, reduces to Eqs. (A63) and (A63).

$$0 = \alpha D_{O_2} P_{50}\left[\nabla'^2 O_2'\right] \tag{A63}$$

$$0 = [NO]^o D_{NO}\left[\nabla'^2 [NO]'\right] \tag{A64}$$

The mass balances for the endothelial and smooth muscle layers were nondimensionalized as well. However, the reaction rates describing the rate of O_2 and NO consumption and NO production are dependent on the dimensional value of the pO_2 because $R_{NO,max}$, Q_{max}, and k_{sm} are dimensional constants. The pO_2 must remain dimensional in these terms and must be in units of mm Hg in order to produce the correct values.

The dimensional rate equations, Eqs. (A65.a) and (A65.b), for the endothelial wall are:

$$R_{O_2} = -R_{NO,max}\frac{pO_2}{pO_2 + K_m} \tag{A65.a}$$

$$R_{NO} = R_{NO,max}\frac{pO_2}{pO_2 + K_m} \tag{A65.b}$$

And the rate equations, Eqs. (A66) and (A67), for the smooth muscle layer are:

$$R_{O_2} = -Q_{max}\frac{pO_2}{pO_2 + \left(K_{sm}\left(1+\frac{[NO]}{27nm}\right)\right)} \tag{A66}$$

$$R_{NO} = -k_{sm}[NO] \tag{A67}$$

By scaling only the non-rate terms, the endothelial wall governing equations for pO_2 and NO become:

$$0 = \alpha D_{O_2} P_{50}\left[\nabla'^2 pO_2'\right] - R_{NO,max}\frac{pO_2}{pO_2 + K_m} \tag{A68}$$

$$0 = [NO]^o D_{NO}\left[\nabla'^2 [NO]'\right] + R_{NO,max}\frac{pO_2}{pO_2 + K_m} \tag{A69}$$

Similarly the balances in the smooth muscle regions are:

$$0 = \alpha D_{O_2} P_{50}\left[\nabla'^2 O_2'\right] - Q_{max}\frac{pO_2}{pO_2 + \left(K_m\left(1+\frac{[NO]}{27nm}\right)\right)} \tag{A70}$$

$$0 = [NO]^o D_{NO}\left[\nabla'^2 [NO]'\right] - k_{sm}[NO]^2 \tag{A70}$$

Appendix B. Boundary conditions

The inlet pO_2 (at $z=0$) is an adjustable model parameter in these simulations. The remaining boundary conditions consist of convective flux of NO at the inlet of the arteriole, convective flux of O_2 and NO at the outlet of the arteriole ($z=L$), axial symmetry at the center of the arteriole ($r=0$), and continuity of O_2 and NO was applied between the core-plasma and plasma-glycocalyx regions. The convective flux boundary condition was applied at $z=L$ in the arteriole, since it assumes that all endothelial and tissue cells are absent and therefore no O_2 can be consumed at that boundary. Continuity boundary conditions were used for O_2 and NO at the boundaries between each region at $r=r_c$, r_w and r_i. The isolated symmetry boundary condition was applied to both ends of the capillary, $z=0$ and $z=L$, and at the tissue edge, R_T.

The boundary conditions for the NO and O_2 transport model are presented below in terms of the nondimensional parameters. Please refer to Table 2 and Fig. 2 for references to specific r and z values.

1) There is radial symmetry at the center of the arteriole, Eq. (B1).

$$\frac{\partial pO_2'}{\partial r'}\Big|_{r'=0} = \frac{\partial NO'}{\partial r'}\Big|_{r'=0} = \frac{\partial S_{RBC}}{\partial r'}\Big|_{r'=0} = \frac{\partial S_{HBOC}}{\partial r'}\Big|_{r'=0} = 0 \tag{B1}$$

2) The arteriole inlet pO_2 is constant, Eq. (B2), and there is only nondiffusive flux of NO at the inlet, Eq. (B3). The fractional saturation of RBC Hb and HBOCs were determined from the Adair and Hill equations (Appendix D), respectively, at the given inlet pO_2, Eqs. (B4) and (B5).

$$pO_2'\big|_{0\le r'\le r_2, z'=0} = \frac{pO_{2,inlet}}{P_{50}} \tag{B2}$$

$$-D_{NO}\nabla NO'\big|_{0\le r'\le r_2, z'=0} = 0 \tag{B3}$$

$$S_{RBC}\big|_{0\le r'\le r_2, z'=0} = Y_{e,RBC\ @\ pO_{2,inlet}} \tag{B4}$$

$$S_{HBOC}\big|_{0\le r'\le r_2, z'=0} = Y_{e,HBOC\ @\ pO_{2,inlet}} \tag{B5}$$

3) All closed boundaries are considered isolated, thus there is no flux of any species out of the closed boundaries, Eqs. (B6)–(B8). Since RBCs and HBOCs are contained inside the arteriole space, there is no flux of either past the plasma region, r_2.

$$\nabla pO'_2\big|_{r_2\le r'\le R_{T2}, z'=0} = \nabla pO_2'\big|_{r_2\le r'\le R_{T2}, z'=1} = \nabla pO_2'\big|_{r=r_T, 0\le z'\le 1} = 0 \tag{B6}$$

$$\nabla NO'\big|_{r_2\le r'\le R_{T2}, z'=0} = \nabla NO'\big|_{r_2\le r'\le R_{T2}, z'=1} = \nabla NO'\big|_{r=r_T, 0\le z'\le 1} = 0 \tag{B7}$$

$$\nabla S_{RBC}\big|_{0\le r'\le r_2, z'=1} = \nabla S_{RBC}\big|_{r=r_2, 0\le z'\le 1} = \nabla S_{HBOC}\big|_{0\le r'\le r_2, z'=1} = \nabla S_{HBOC}\big|_{r=r_2, 0\le z'\le 1} = 0 \tag{B8}$$

4) There is no flux of Mb across any tissue space boundary; Mb is completely contained in the tissue region.

5) The O_2 tension and NO concentration are continuous across all interior boundaries (core-plasma, plasma-glycocalyx, glycocalyx-wall, etc.)

Appendix C. Hb and hematocrit profiles

Since the RBCs pack into a core region in the center of the arteriole lumen, the core *hct* will be much higher than the overall *hct* (or discharge *hct*) and the concentration of RBCs will decrease further away from the core region. The concentration of HBOCs at any given location is restrained to be in the plasma space (any place there is not a RBC) within the fractional volume $(1-hct)$ (i.e. an HBOC cannot penetrate into a RBC) [23]. In this work, it is useful to define the discharge *hct*, H_D, which is the total volume of RBCs divided by the total volume of blood (RBCs and plasma) [23,27]. In our work, H_D was varied between simulations.

Chen et al. developed a simulation using three different hematocrit profiles (step, linear and parabolic) to define the local *hct* at a given *r* [27]. According to Chen et al.'s reported results, simulations using a linear *hct* profile yielded the best agreement with experimental results. Due to these favorable results, our simulations employed a linear *hct* profile, Eq. (C1).

$$hct(r) = \begin{cases} H_c & 0<r<r_1 \\ H_c \dfrac{r_2 - r}{r_2 - r_1} & r_1<r<r_2 \end{cases} \tag{C1}$$

The core hematocrit, H_c, is a function of the radius of the core region, arteriole radius, H_D, and the velocity profile. It is determined from a simple RBC mass balance in the arteriole space, Eq. (C2). The radius of the RBC-rich core (r_1) is dependent on the total RBC hematocrit (H_D) as described by Cole et al. and Tateishi et al. [31,32]. The values for the CR fraction of the arteriole lumen are listed in Table 2.

$$2\pi \int_0^{r_2} hct(r) v_z r dr = 2\pi H_D \int_0^{r_2} v_z r dr \tag{C2}$$

Due to the varying *hct*, the local Hb concentration will also depend on the radius via the *hct* by $[Hb_{total}] = [Hb_{cell}]hct$. Where $[Hb_{cell}]$ is the Hb concentration inside a RBC. The overall HBOC concentration was varied between simulations. Therefore, the local HBOC concentration was defined from the overall HBOC concentration, H_D and the local *hct*, Eq. (C3). The factor $1/(1-H_D)$ adjusts the $[HBOC_{overall}]$ to a concentration limited to just the plasma space. The factor $(1-hct)$ accounts for the local $[HBOC_{total}]$ due to the RBC *hct* profile.

$$[HBOC_{total}] = [HBOC_{overall}] \frac{1 - hct}{1 - H_D} \tag{C3}$$

Where H_D = discharge *Hct*.

Appendix D. Other biophysical parameters

In the transport equations, the diffusion coefficient of O_2 within each region (D_{O_2}) is dependent on the Hb concentration as described by Patton et al. and Bouwer et al. [21,48], Eq. (D1). Also the diffusivity of Hb is dependent on its own concentration as well, Eq. (D2).

$$D_{O_2} = 2.77 \times 10^{-5} \left(1 - \frac{[Hb]}{100}\right) 10^{-[Hb]/119} \tag{D1}$$

$$D_{Hb} \text{ or } D_{HBOC} = 9.74 \times 10^{-7} \left(1 - \frac{[Hb]}{46}\right) 10^{-[Hb]/128} \tag{D2}$$

The velocity profile was also described by Chen et al. and is assumed to consist of plug flow in the RBC rich core with a linearly decreasing velocity profile with increasing *r* in the cell-depleted plasma region [27], Eq. (D3).

$$v_z = \begin{cases} U_{avg} & 0<r<r_1 \\ U_{avg} \dfrac{r - r_2}{r_1 - r_2} & r_1<r<r_2 \end{cases} \tag{D3}$$

The diffusivity of Hb and HBOC was assumed to be dependent on the molecular weight according to:

$$D_{Hb} = 1.013 \times 10^{-4} (\text{molecular weight})^{-0.46} \tag{D4}$$

The dissociation rate constants for oxyHb within RBCs at 37 °C were reported by Vadapalli et al. and Patton et al. [21,25]. The dissociation rate constants for other HBOCs were based on previously determined rate constants. However, most of these rate constants were determined at 20 °C. Therefore, the dissociation rate constant at 37 °C was determined using the Arrhenius relationship assuming activation energies of wild type Hb.

The O_2–Hb equilibrium relationship in RBCs was described mathematically by the four-step Adair model with Y_e representing the fractional saturation of oxyHb. Hence, the Adair model, Eq. (D5), allows us to relate the O_2 tension to the Hb saturation at equilibrium.

$$Y_e = \frac{A_1 pO_2 + 2A_2 pO_2^2 + 3A_3 pO_2^3 + 4A_4 pO_2^4}{4(1 + A_1 pO_2 + A_2 pO_2^2 + A_3 pO_2^3 + A_4 pO_2^4)} \tag{D5}$$

The O_2–HBOC equilibrium relationship was described by the single-step Hill equation, Eq. (D6). Again Y_e is the fractional saturation of oxyHBOC.

$$Y_e = \frac{pO_2^n}{pO_2^n + P_{50}^n} \tag{D6}$$

Appendix E. Supplementary data

Supplementary data associated with this article can be found, in the online version, at doi:10.1016/j.bpc.2009.02.005.

References

[1] A.G. Tsai, K.D. Vandegriff, M. Intaglietta, R.M. Winslow, Targeted O_2 delivery by low-P_{50} hemoglobin: a new basis for O_2 therapeutics, Am. J. Physiol, Heart Circ. Physiol. 285 (2003) H1411–H1419.
[2] R.M. Winslow, J. Lohman, A. Malavalli, K.D. Vandegriff, Comparison of PEG-modified albumin and hemoglobin in extreme hemodilution in the rat, J. Appl. Physiol. 97 (2004) 1527–1534.
[3] D.H. Doherty, M.P. Doyle, S.R. Curry, R.J. Vali, T.J. Fattor, J.S. Olson, D.D. Lemon, Rate of reaction with nitric oxide determines the hypertensive effect of cell-free hemoglobin, Nat. Biotechnol. 16 (1998) 672–676.
[4] J.S. Olson, E.W. Foley, C. Rogge, A. Tsai, M.P. Doyle, D.D. Lemon, NO scavenging and the hypertensive effect of hemoglobin-based blood substitutes, Free Radic. Biol. Med. 36 (2004) 685–697.
[5] J.G. Riess, Oxygen carriers ("blood substitutes")—raison d'etre, chemistry, and some physiology, Chem. Rev. 101 (2001) 2797–2919.
[6] P. Condorelli, S.C. George, In vivo control of soluble guanylate cyclase activation by nitric oxide: a kinetic analysis, Biophys. J. 80 (2001) 2110–2119.
[7] A. Popel, M. Kavdia, N.M. Tsoukias, in: K. Kobayashi, E. Tsuchida, H. Horinouchi (Eds.), Artificial Oxygen Carrier, Effect of Hemoglobin-Based Blood Substitutes on Nitric Oxide Transport: Mathematical Models, vol. 12, Springer, Tokyo, 2005, pp. 176–185.
[8] N.M. Tsoukias, M. Kavdia, A.S. Popel, A theoretical model of nitric oxide transport in arterioles: frequency- vs. amplitude-dependent control of cGMP formation, Am. J. Physiol, Heart Circ. Physiol. 286 (2004) H1043–H1056.
[9] M. Kavdia, N.M. Tsoukias, A.S. Popel, Model of nitric oxide diffusion in an arteriole: impact of hemoglobin-based blood substitutes, Am. J. Physiol, Heart Circ. Physiol. 282 (2002) H2245–H2253.
[10] M. Kavdia, A.S. Popel, Contribution of nNOS- and eNOS-derived NO to microvascular smooth muscle NO exposure, J. Appl. Physiol. 97 (2004) 293–301.
[11] W.K. Alderton, C.E. Cooper, R.G. Knowles, Nitric oxide synthases: structure, function and inhibition, Biochem. J 357 (2001) 593–615.
[12] O.W. Griffith, D.J. Stuehr, Nitric oxide synthases: properties and catalytic mechanism, Annu. Rev. Physiol. 57 (1995) 707–736.

[13] D.G. Buerk, Can we model nitric oxide biotransport? A survey of mathematical models for a simple diatomic molecule with surprisingly complex biological activities, Annu. Rev. Biomed. Eng. 3 (2001) 109–143.
[14] K.J. Chen, R.N. Pittman, A.S. Popel, Nitric oxide in the vasculature: where does it come from and where does it go? A quantitative perspective, Antioxid. Redox Signal. 10 (2008) 1185–1198.
[15] K.D. Vandegriff, A. Malavalli, J. Wooldridge, J. Lohman, R.M. Winslow, MP4, a new nonvasoactive PEG-Hb conjugate, Transfusion 43 (2003) 509–516.
[16] K.D. Vandegriff, A. Bellelli, M. Samaja, A. Malavalli, M. Brunori, R.M. Winslow, Kinetics of NO and O_2 binding to a maleimide poly(ethylene glycol)conjugated human haemoglobin, Biochem. J 382 (2004) 183–189.
[17] K.D. Vandegriff, A. Malavalli, C. Minn, E. Jiang, J. Lohman, M.A. Young, M. Samaja, R.M. Winslow, Oxidation and haem loss kinetics of poly(ethylene glycol)-conjugated haemoglobin (MP4): dissociation between in vitro and in vivo oxidation rates, Biochem. J 399 (2006) 463–471.
[18] P.W. Buehler, R.A. Boykins, Y.P. Jia, S. Norris, D.I. Freedberg, A.I. Alayash, Structural and functional characterization of glutaraldehyde-polymerized bovine hemoglobin and its isolated fractions, Anal. Chem. 77 (2005) 3466–3478.
[19] A.I. Alayash, A.G. Summers, F. Wood, Y.P. Jia, Effects of glutaraldehyde polymerization on oxygen transport and redox properties of bovine hemoglobin, Arch. Biochem. Biophys. 391 (2001) 225–234.
[20] J.C. Hartman, G. Argoudelis, D. Doherty, D. Lemon, R. Gorczynski, Reduced nitric oxide reactivity of a new recombinant human hemoglobin attenuates gastric dysmotility, Eur. J. Pharmacol. 363 (1998) 175–178.
[21] J.N. Patton, A.F. Palmer, Numerical simulation of oxygen delivery to muscle tissue in the presence of hemoglobin-based oxygen carriers, Biotechnol. Progr. 22 (2006) 1025–1049.
[22] D.R. Arifin, A.F. Palmer, Determination of size distribution and encapsulation efficiency of liposome-encapsulated hemoglobin blood substitutes using asymmetric flow field-flow fractionation coupled with multi-angle static light scattering, Biotechnol. Progr. 19 (2003) 1798–1811.
[23] M. Kavdia, A.S. Popel, Wall shear stress differentially affects NO level in arterioles for volume expanders and Hb-based O_2 carriers, Microvasc. Res. 66 (2003) 49–58.
[24] A.S. Popel, Theory of oxygen transport to tissue, Crit. Rev. Biomed. Eng. 17 (1989) 257–321.
[25] A. Vadapalli, D. Goldman, A.S. Popel, Calculation of oxygen transport by red blood cells and hemoglobin solutions in capillaries, Artif. Cells Blood Substit. Immobil. Biotechnol. 30 (2002) 157–188.
[26] P.K. Nair, J.D. Hellums, J.S. Olson, Prediction of oxygen-transport rates in blood flowing in large capillaries, Microvasc. Res. 38 (1989) 269–285.
[27] X.W. Chen, D. Jaron, K.A. Barbee, D.G. Buerk, The influence of radial RBC distribution, blood velocity profiles, and glycocalyx on coupled NO/O_2 transport, J. Appl. Physiol. 100 (2006) 482–492.
[28] M.R. King, D.T. Leighton, Measurement of shear-induced dispersion in a dilute emulsion, Phys. Fluids 13 (2001) 397–406.
[29] R. Zhou, H.-C. Chang, Wetting penetration failure of blood suspensions, J. Colloid Interface Sci. 287 (2005) 647–656.
[30] R.H. Zhou, J. Gordon, A.F. Palmer, H.C. Chang, Role of erythrocyte deformability during capillary wetting, Biotechnol. Bioeng. 93 (2006) 201–211.
[31] R.H. Cole, K.D. Vandegriff, A.J. Szeri, O. Savas, D.A. Baker, R.M. Winslow, A quantitative framework for the design of acellular hemoglobins as blood substitutes: Implications of dynamic flow conditions, Biophys. Chem. 128 (2007) 63–74.
[32] N. Tateishi, Y. Suzuki, I. Cicha, N. Maeda, O_2 release from erythrocytes flowing in a narrow O_2-permeable tube: effects of erythrocyte aggregation, Am. J. Physiol, Heart Circ. Physiol. 281 (2001) H448–H456.
[33] R.L. Fournier, Basic Transport Phenomena in Biomedical Engineering, Taylor & Francis, Philadelphia, PA, 1999.
[34] A.S. Popel, D. Goldman, A. Vadapalli, in: J.F. Dunn, H.M. Swartz (Eds.), In Oxygen Transport to Tissue XXIV, Modeling of Oxygen Diffusion from the Blood Vessels to Intracellular Organelles, vol. 530, Kluwer Academic/Plenum Publishers, New York, NY, 2003, pp. 485–495.
[35] A.G. Tsai, P. Cabrales, B.N. Manjula, S.A. Acharya, R.M. Winslow, M. Intaglietta, Dissociation of local nitric oxide concentration and vasoconstriction in the presence of cell-free hemoglobin oxygen carrier, Blood 108 (2006) 3603–3610.
[36] K.A. Lamkin-Kennard, D.G. Buerk, D. Jaron, Interactions between NO and O_2 in the microcirculation: a mathematical analysis, Microvasc. Res. 68 (2004) 38–50.
[37] J.R. Stone, R.H. Sands, W.R. Dunham, M.A. Marletta, Spectral and ligand-binding properties of an unusual hemoprotein, the ferric form of soluble guanylate cyclase, Biochemistry 35 (1996) 3258–3262.
[38] M.L. Dimino, A.F. Palmer, Hemoglobin-based O_2 carrier O_2 affinity and capillary inlet pO_2 are important factors that influence O_2 transport in a capillary, Biotechnol. Progr. 23 (2007) 921–931.
[39] S.I. Gundersen, A.F. Palmer, Conjugation of methoxypolyethylene glycol to the surface of bovine red blood cells, Biotechnol. Bioeng. 96 (2007) 1199–1210.
[40] R.M. Winslow, Blood substitutes, Adv. Drug Deliv. Rev. 40 (2000) 131–142.
[41] R.M. Winslow, Current status of blood substitute research: towards a new paradigm, J. Intern. Med. 253 (2003) 508–517.
[42] P. Cabrales, A.G. Tsai, M. Intaglietta, Nitric oxide regulation of microvascular oxygen exchange during hypoxia and hyperoxia, J. Appl. Physiol. 100 (2006) 1181–1187.
[43] B.Y.S. Váquez, P. Cabrales, A.G. Tsai, P.C. Johnson, M. Intaglietta, Lowering of blood pressure by increasing hematocrit with non-nitric oxide-scavenging red blood cells, Am. J. Respir. Cell Mol. Biol. 38 (2008) 135–142.
[44] J. Martini, B. Carpentier, A.C. Negrete, J.A. Frangos, M. Intaglietta, Paradoxical hypotension following increased hematocrit and blood viscosity, Am. J. Physiol, Heart Circ. Physiol. 289 (2005) H2136–H2143.
[45] B. Yu, M.J. Raher, G.P. Volpato, K.D. Bloch, F. Ichinose, W.M. Zapol, Inhaled nitric oxide enables artificial blood transfusion without hypertension, Circulation 117 (2008) 1982–1990.
[46] D. Voet, J.G. Voet, Biochemistry, John Wiley & Sons, Inc., New York, 1995.
[47] X.W. Chen, D.G. Buerk, K.A. Barbee, D. Jaron, A model of NO/O_2 transport in capillary-perfused tissue containing an arteriole and venule pair, Ann. Biomed. Eng. 35 (2007) 517–529.
[48] S.T. Bouwer, L. Hoofd, F. Kreuzer, Diffusion coefficients of oxygen and hemoglobin measured by facilitated oxygen diffusion through hemoglobin solutions, Biochim. Biophys. Acta, Prot. Struct. Mol. Enzymol. 1338 (1997) 127–136.